ISA Transactions 152 (2024) 113–128

Contents lists available at ScienceDirect

ISA Transactions

journal homepage: www.elsevier.com/locate/isatrans

Research article

A fault isolation strategy for industrial processes using outlier-degree-based variable contributions

Lingxia Mu [a], Wenzhe Sun [a], Youmin Zhang [b,*], Nan Feng [c,*], Xianghong Xue [a], Qingliang Li [a]

[a] Shaanxi Key Laboratory of Complex System Control and Intelligent Information Processing, Xi'an University of Technology, Xi'an, Shaanxi 710048, China
[b] Department of Mechanical, Industrial & Aerospace Engineering, Concordia University, Montreal, Quebec H3G 1M8, Canada
[c] School of Intelligence Science and Technology, University of Science and Technology Beijing, Beijing 100083, China

ARTICLE INFO

Keywords:
Fault isolation
Improved k-nearest neighbor rule
Variable contribution
Isolation threshold value

ABSTRACT

In industrial process monitoring, it is always a challenging and practical problem to analyze the causes of the system fault by isolating true fault variables from vast amounts of process data. However, the phenomenon of smearing effect occurs by using the traditional contribution analysis-based isolation methods since the defined isolation indices of different variables affect each other. In this paper, a new fault isolation method is proposed based on local outlier factor and improved k-nearest neighbor rule aiming to improve the isolation accuracy. Firstly, the nearest neighbors of each sample are obtained along the direction of a specific variable. Based on the nearest neighbors, the outlier-degree value of the variable is calculated and regarded as the contribution of the variable. Then, the contribution of the variable in all samples are obtained in the same way, among which the maximum one is selected as the isolation threshold value of this variable. During the online monitoring, the contribution of the variable in the newly collected sample is calculated in real time. Once the contribution is greater than the threshold, the variable is judged to be the dominant factor causing the system fault. Two cases on numerical example and Tennessee Eastman process are conducted to evaluate the effectiveness of the proposed method.

1. Introduction

The monitoring of the process variables is of great significance for regulating working conditions and ensuring product quality in industrial processes. In the field of process monitoring, fault detection, fault isolation, fault diagnosis, and fault prognosis are usually studied. Fault isolation involves identifying certain variables causing a fault from all monitored variables after the fault is detected [1–3].

The traditional fault isolation method is based on contribution analysis (CA) in the framework of principle component analysis (PCA) [4–9], including complete decomposition contribution (CDC), reconstruction-based contribution (RBC), partial decomposition contribution (PDC), diagonal contribution (DC), and angle-based contribution (ABC) [10–13]. In these CA-based fault isolation methods, data is generally by assuming to follow a specific distribution. For instance, it is assumed that data obey multidimensional Gaussian distribution. However, it is hard to meet the Gaussian distribution condition in practice. On the other hand, variable contributions are constructed to isolate the fault variable from the monitored data. Generally, variable contributions are computed by indicators like Hotelling's T-squared (T^2), squared prediction error (SPE), and the combined index φ. Then, the variable with the biggest contribution value is regarded as the fault variable. However, it is illustrated that inaccurate isolation may occur in the traditional CA-based isolation methods. The reason is that the contribution magnitude of fault-free variables may be amplified since the computation of the variable contribution is related with all the original variables. This is the so-called phenomenon of the smearing effect [14]. For example, in fault case, the change of certain variable might affect the contribution value of the other normal variables. This leads to the possibility that the contributions of the affected normal variables may exceed that of the true fault variables, thereby resulting in inaccurate isolation [15].

Hence, to reduce the negative impact of smearing effect on isolation results in the CA-based methods, some improved methods are proposed. In [6], an adaptive PCA-based detection and isolation method is designed for incipient faults, which is suitable for non-Gaussian industrial fault type and has high isolation efficiency. In [16], a modified isolation approach based on distributed kernel principal component

* Corresponding authors.
E-mail addresses: ymzhang@encs.concordia.ca (Y. Zhang), fengnan_fn@163.com (N. Feng).

https://doi.org/10.1016/j.isatra.2024.06.007
Received 16 April 2023; Received in revised form 6 June 2024; Accepted 6 June 2024
Available online 7 June 2024

regression (DKPCR) is proposed, which can quickly isolate the fault-related variables by alleviating the smearing effect. In [17], a new dynamic PCA-based fault detection and isolation method is proposed where the fault is isolated by calculating the variable relative contribution. In [18], a novel fault detection and isolation approach based on the structured joint sparse PCA is designed, where a new score index is used to locate and isolate fault variable. However, misdiagnosis still occurs in above mentioned methods since the problem of smearing effect cannot be fundamentally solved due to the inherent characteristic of the CA-based isolation methods. In addition, the fault isolation ability in the presence of multiple fault variables is not considered in the above traditional CA-based methods. Furthermore, the isolation threshold is not defined for the variable contribution, which may lead to ambiguous decisions.

To overcome the above issues, some new data-driven methods are proposed [19–24]. In [21], a neural networks-based method is designed with application to internal combustion engine fault isolation. Both single fault variable and multiple fault variables can be accurately detected and isolated. However, a large amount of prior information about fault is hard to obtain for the model training. In [23], k-nearest neighbor (kNN) reconstruction is proposed for fault isolation, which combines the kNN-based prediction and reconstruction-based method to enhance isolability of the fault variable. But these methods lack theoretical analysis of the isolability. In [24], a fault isolation scheme using classification and regression tree is proposed, which is applied for steam boilers to isolate fault variables. As a supervised machine learning-based method, lots of prior information about the process fault are needed for the training of the model. However, in the practical industrial process, unknown faults become more likely to occur. The prior fault information is usually difficult to obtain. Furthermore, theoretical analysis of the isolability is necessary for the isolation method.

In this paper, a new isolation method using outlier-degree-based variable contributions is proposed. The smearing effect can be eliminated, and the isolation accuracy is improved using the proposed method. In addition, no prior information of the fault is required. Hence the proposed method can be potentially applied to a more practical industrial scenario. Furthermore, detailed theoretical analysis of isolability for fault variables is also provided in both cases of single and multiple fault variables. The numerical example and Tennessee Eastman (TE) process are used to demonstrate the performance of proposed method. The results indicate that the proposed method can efficiently isolate fault variables. The main contributions of this paper are as follows.

1) A new fault isolation strategy is proposed where variable contribution is defined from the perspective of the spatial distance between variables. This idea is different from the traditional CA-based methods where the contribution indicator of variables is prone to interfere with each other. In the proposed method, a new contribution indicator defined in the original measurement space is used to evaluate the likelihood that a variable is a faulty variable. And the isolation threshold value of the variable contribution is explicitly proposed which is more convenient to make the decision for fault variable isolation.
2) The variable contribution is obtained by calculating the outlier-degree relative to the k-nearest neighbor of the variable. The nearest neighbors are searched along the direction of a specific variable with improved k-nearest neighbor (IkNN) rather than in the whole space of the sample with the kNN, which can significantly reduce computational complexity.
3) The proposed method can be applied to the cases of single and multiple fault variables. In both cases, detailed theoretical analysis of isolability for fault variables is given. Case studies on numerical examples and TE process are also provided. The effectiveness of the proposed method is demonstrated theoretically and experimentally.

The remainder of this paper is organized as follows. The introduction of fault isolation based on CA methods, local outlier factor algorithm, kNN algorithm, and IkNN algorithm are given in Section 2, respectively. The main content of the proposed isolation strategy is given in Section 3. Detailed theoretical derivation and analysis of the isolability for fault variables are provided in Section 4. Simulations on the numerical example and TE process are conducted to verify the isolating performance of the proposed method in Section 5. Section 6 concludes the paper.

2. Preliminaries

In this section, fault isolation based on contribution analysis methods, local outlier factor algorithm, and k-nearest neighbor algorithm are introduced. Besides, an improved k-nearest neighbor algorithm is proposed. The key ideas of the local outlier factor algorithm and improved k-nearest neighbor algorithm are used in the following proposed fault isolation method.

2.1. Fault isolation based on CA methods

The CA methods are defined based on the fault detection indices of PCA. The true faulty variables can be identified by computing a quantity which represents the contribution from each variable to the indices. The fault detection indices of PCA are introduced first.

Given the dataset matrix $\boldsymbol{X} = \left[\boldsymbol{X}^1, \ldots, \boldsymbol{X}^n\right]^T \in R^{n\times m}$ consisting of n samples, each sample $\boldsymbol{X}^i = \left(x_1^i, \ldots, x_m^i\right)$ is composed of m measured variables. Each variable in $\boldsymbol{X}$ is usually scaled to zero mean and unit variance. Then, the covariance matrix $\boldsymbol{S}$ is decomposed by eigenvalue decomposition, obtaining.

$$\boldsymbol{S} = \frac{1}{n-1}\boldsymbol{X}^T\boldsymbol{X} = \begin{bmatrix}\boldsymbol{P} & \widetilde{\boldsymbol{P}}\end{bmatrix}\begin{bmatrix}\boldsymbol{\Lambda} & \boldsymbol{0} \\ \boldsymbol{0} & \widetilde{\boldsymbol{\Lambda}}\end{bmatrix}\begin{bmatrix}\boldsymbol{P} & \widetilde{\boldsymbol{P}}\end{bmatrix}^T \tag{1}$$

where the columns of $\boldsymbol{P} \in R^{m\times l}$ are associated with the first l largest eigenvalues of diagonal matrix $\boldsymbol{\Lambda} \in R^{l\times l}$, and the columns of $\widetilde{\boldsymbol{P}} \in R^{m\times(m-l)}$ are associated with the rest $(m-l)$ largest eigenvalues of diagonal matrix $\widetilde{\boldsymbol{\Lambda}} \in R^{(m-l)\times(m-l)}$.

The commonly used detection indices of PCA are T^2, SPE, and the combined index φ. For simplicity, a unified index is introduced [14].

$$Index(\boldsymbol{x}) = \left\|\boldsymbol{M}^{1/2}\boldsymbol{x}\right\|_2^2 \quad = \quad \boldsymbol{x}^T\boldsymbol{M}\boldsymbol{x}. \tag{2}$$

This unified index becomes T^2, SPE, and combined index φ when $\boldsymbol{M} = \boldsymbol{P}\boldsymbol{\Lambda}^{-1}\boldsymbol{P}^T$, $\boldsymbol{M} = \widetilde{\boldsymbol{P}}\widetilde{\boldsymbol{P}}^T$, and $\boldsymbol{M} = \boldsymbol{P}\boldsymbol{\Lambda}^{-1}\boldsymbol{P}^T/\tau^2 + \widetilde{\boldsymbol{P}}\widetilde{\boldsymbol{P}}^T/\delta^2$, respectively, where τ^2 and δ^2 are control limit of T^2 and SPE, respectively [12]. Next, two typical fault isolation methods based on CA are briefly introduced.

1) CDC: The unified formula of CDC is defined as [12].

$$\mathrm{CDC}_i(\boldsymbol{x}) = \left(\xi_i^T\boldsymbol{M}^{1/2}\boldsymbol{x}\right)^2 \tag{3}$$

where ξ_i is the ith column of identity matrix. The sum of CDC_i is equal to the corresponding detection index, i.e., $\sum_{i=1}^{m}\mathrm{CDC}_i(\boldsymbol{x}) = \mathrm{Index}(\boldsymbol{x})$.

2) RBC: The variable contributions are defined as the amount of the reconstruction of indices along with one of the variable directions, and more detailed information about RBC can be found in [15].

$$\mathrm{RBC}_i(\boldsymbol{x}) = \left(\xi_i^T\boldsymbol{M}\boldsymbol{x}\right)^2 \Big/ \xi_i^T\boldsymbol{M}\xi_i \tag{4}$$

where ξ_i is a possible fault direction.

However, from the definitions in Eqs. (3) and (4), it can be inferred that any change of a variable can cause changes of all the variable contributions because the defined variable contribution is related to all the original variables. This is the so-called phenomenon of smearing effect, which would lead to misdiagnosis.

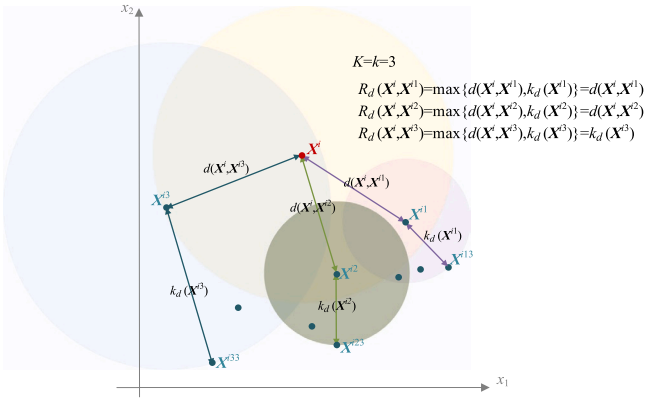

Fig. 1. Schematic diagram of the reachable distance R_d (K= k = 3).

2.2. Local outlier factor (LOF) algorithm

The LOF method is an outlier detection algorithm based on relative density, which uses local outlier factor index to measure the outlier degree of the sample [25]. It is widely used for fault detection in industrial processes [26–29]. Given the dataset matrix $\boldsymbol{X} = \left[\boldsymbol{X}^1, \ldots, \boldsymbol{X}^n\right]^T \in R^{n\times m}$ consisting of n samples, where each sample $\boldsymbol{X}^i = (x_1^i, \ldots, x_m^i)$ is composed of m measured variables, the principle of LOF algorithm is as follows.

(1) The nearest neighbors of sample $\boldsymbol{X}^i$ in dataset matrix $\boldsymbol{X}$ is searched based on the Euclidean distance, achieving the dataset $N(\boldsymbol{X}^i)$

$$N(\boldsymbol{X}^i) = \left[\boldsymbol{X}^{i1}, \boldsymbol{X}^{i2}, \ldots, \boldsymbol{X}^{il}, \ldots, \boldsymbol{X}^{iK}\right]^T, \quad l = 1, 2, \ldots, K \tag{5}$$

where K is a hyperparameter denoting the number of the nearest neighbors of $\boldsymbol{X}^i$. In addition, the Euclidean distance between $\boldsymbol{X}^i$ and $\boldsymbol{X}^{il}$ is defined by $d(\boldsymbol{X}^i, \boldsymbol{X}^{il})$

$$d(\boldsymbol{X}^i, \boldsymbol{X}^{il}) = \sqrt{\sum_{j=1}^{n}\left(x_j^i - x_j^{il}\right)^2}, \quad j = 1, 2, \ldots, m \tag{6}$$

where x_j^i is jth variable in sample $\boldsymbol{X}^i$ and x_j^{il} is the jth variable of sample $\boldsymbol{X}^{il}$..

(2) The nearest neighbor sets of $\boldsymbol{X}^{il}$ can be obtained by the same way. The kth distance of $\boldsymbol{X}^{il}$, $k_d(\boldsymbol{X}^{il})$, is Euclidean distance between $\boldsymbol{X}^{il}$ and its kth nearest neighbor $\boldsymbol{X}^{ilk}$, given as

$$k_d(\boldsymbol{X}^{il}) = \sqrt{\sum_{j=1}^{n}\left(x_j^{il} - x_j^{ilk}\right)^2} \tag{7}$$

(3) Then, the reachable distance R_d from $\boldsymbol{X}^i$ to each nearest neighbor sample in $N(\boldsymbol{X}^i)$ is calculated by

$$R_d(\boldsymbol{X}^i, \boldsymbol{X}^{il}) = \max\{d(\boldsymbol{X}^i, \boldsymbol{X}^{il}), k_d(\boldsymbol{X}^{il})\} \tag{8}$$

For convenience of the description of the above distances, Fig. 1 is presented where K and k are both set to be 3. The sample $\boldsymbol{X}^{i1}$, $\boldsymbol{X}^{i2}$, and $\boldsymbol{X}^{i3}$, are the three nearest neighbors of sample $\boldsymbol{X}^i$, respectively. Then, $d(\boldsymbol{X}^i, \boldsymbol{X}^{i1})$, $d(\boldsymbol{X}^i, \boldsymbol{X}^{i2})$ and $d(\boldsymbol{X}^i, \boldsymbol{X}^{i3})$ are the Euclidean distance between $\boldsymbol{X}^i$ and $\boldsymbol{X}^{i1}$, $\boldsymbol{X}^{i2}$, $\boldsymbol{X}^{i3}$, respectively. Assuming that samples $\boldsymbol{X}^{i13}$, $\boldsymbol{X}^{i23}$, and $\boldsymbol{X}^{i33}$ are the third nearest neighbor of samples $\boldsymbol{X}^{i1}$, $\boldsymbol{X}^{i2}$, and $\boldsymbol{X}^{i3}$, respectively, $k_d(\boldsymbol{X}^{i1})$, $k_d(\boldsymbol{X}^{i2})$, $k_d(\boldsymbol{X}^{i3})$ are obtained as the third distance of $\boldsymbol{X}^{il}$. Finally, the reachable distance $R_d(\boldsymbol{X}^i, \boldsymbol{X}^{il})$ is achieved by selecting the maximum one between $d(\boldsymbol{X}^i, \boldsymbol{X}^{il})$ and $k_d(\boldsymbol{X}^{il})$.

(4) Based on the above distances, the LOF value can be calculated. Firstly, the local reachability density (LRD) ρ for sample $\boldsymbol{X}^i$ is obtained by inverting average of reachable distance

$$\rho(\boldsymbol{X}^i) = \frac{1}{\frac{1}{K}\sum_{l=1}^{K} R_d(\boldsymbol{X}^i, \boldsymbol{X}^{il})} \tag{9}$$

Then, the LOF of sample $\boldsymbol{X}^i$ is calculated by dividing the average LRD of its K neighbors by the LRD of itself, achieving

$$LOF(\boldsymbol{X}^i) = \frac{1}{K}\frac{\Sigma_{l=1}^{K}\rho(\boldsymbol{X}^{il})}{\rho(\boldsymbol{X}^i)} \tag{10}$$

The LOF value of each training sample $\boldsymbol{X}^i, i = 1, \ldots, n$ is calculated by the same way. Usually, for a normal sample, the LOF value is generally less than or close to 1, which means that its local reachable density is close to that of its nearest neighbors. Thus, the sample and its neighbors belong to the same cluster. While, if LOF value of a sample is much greater than 1, it is highly likely that the sample is an outlier.

The distribution of LOF can be determined by kernel density estimation [30,31], and the upper quantile of the distribution corresponding to the confidence α is used as the control limit, C_{LOF}, of the detection model. In real-time fault detection, LOF value of a test sample $\boldsymbol{X}^t$ is firstly calculated by the same method. Then, $LOF(\boldsymbol{X}^t)$ value of the sample is comparing with the control limit C_{LOF}. If $LOF(\boldsymbol{X}^t) > C_{LOF}$, the sample $\boldsymbol{X}^t$ is judged as an abnormal outlier sample.

2.3. kNN algorithm

The kNN rule was initially proposed for the classification problems. It was extensively applied to fault detection in industrial processes [32–34]. For kNN-based fault detection method, the Euclidean distance $d(\boldsymbol{X}^i, \boldsymbol{X}^{il})$ from $\boldsymbol{X}^i$ to each nearest neighbor sample is firstly calculated by the same method as shown in Eq. (6). Then, the mean of the square of Euclidean distance from $\boldsymbol{X}^i$ to its nearest neighbors $\boldsymbol{X}^{il}(l = 1, \ldots, K)$ is calculated by

$$D^2(\boldsymbol{X}^i) = \frac{1}{K}\sum_{l=1}^{K} d^2(\boldsymbol{X}^i, \boldsymbol{X}^{il}) \tag{11}$$

where D^2 is known as the kNN distance of the sample $\boldsymbol{X}^i$.

The D^2 value of each training sample $\boldsymbol{X}^i$ is computed by the same method. The distribution is determined by methods such as kernel density estimation. The upper quantile of the distribution corresponding to the confidence α is used as the control limit D_c^2 of the detection model. In real-time detection, the D^2 value of test sample $\boldsymbol{X}^t$ is computed. Then, $D^2(\boldsymbol{X}^t)$ is compared with control limit D_c^2. If $D^2(\boldsymbol{X}^t) > D_c^2$, the sample $\boldsymbol{X}^t$ is judged as an abnormal sample.

Remark 1. The LOF and kNN algorithms are commonly used for fault detection in industrial processes by measuring distance between normal and fault samples in the measurement space. For fault detection, only the fault samples are detected, while the exact variable leading to the system fault cannot be distinguished. For industrial applications, fault isolation (i.e., the location of fault source) is usually with practical meanings for process operators to improve the process security and product quality by regulating working condition. Hence, the location of the faulty source is of great importance and necessity. In this paper, inspired by the basic idea of LOF and kNN algorithms, we expanded them to isolate the fault variable from sample. Besides, to improve the computational efficiency, the search direction is modified for determining the nearest neighbors in kNN rule.

2.4. Improved kNN algorithm

In traditional kNN rule, the k nearest neighbors of one sample are obtained by calculating and sorting Euclidean distances between samples in training dataset. The Euclidean distance between one sample and

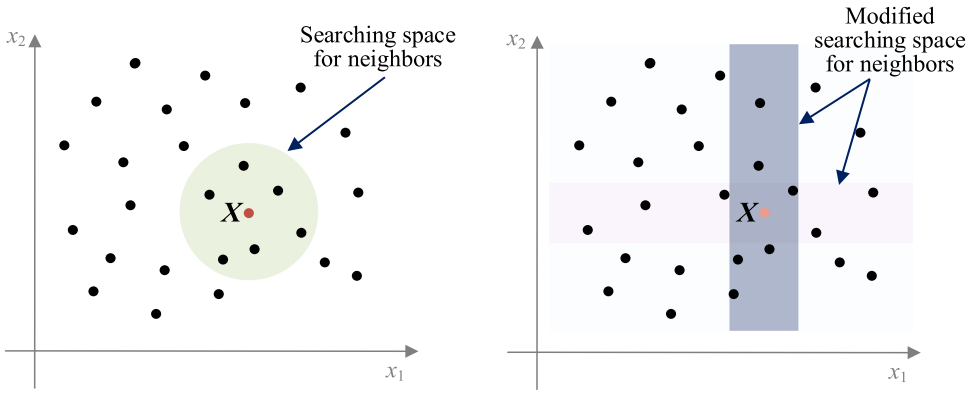

Fig. 2. The difference between kNN rule and IkNN rule ($k = 6$).

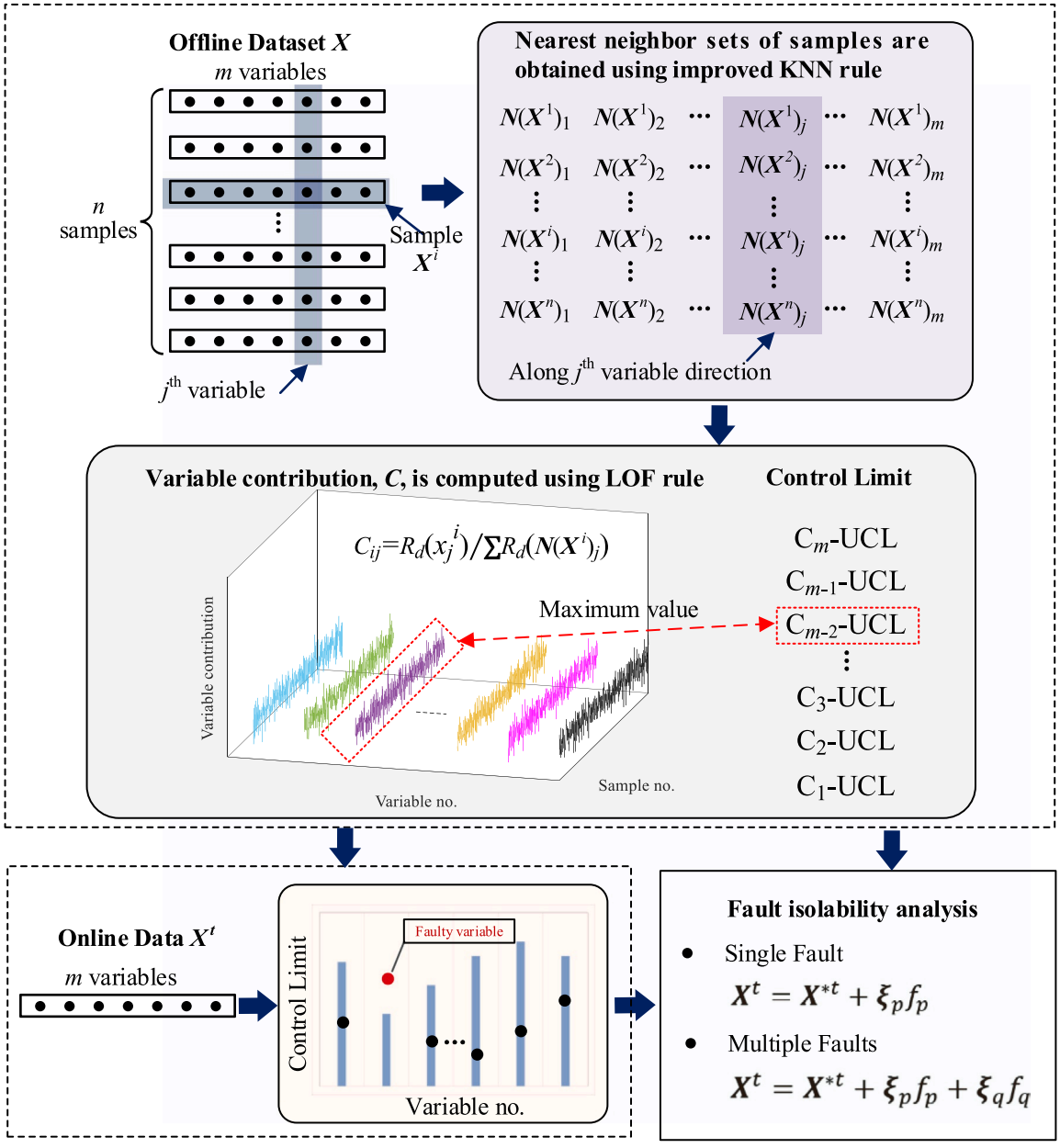

Fig. 3. Block diagram for the proposed fault isolation strategy.

another sample is computed by the sum of squared differences of m variables [32–34]. In this paper, the k nearest neighbors of one sample are searched along the direction of specific variable in the original measurement space. The Euclidean distance between two samples is computed by the squared difference of the specific variable in the two samples.

Taking two-dimensional data as an example, the difference between the traditional kNN rule and improved kNN rule is expressed in Fig. 2. k is set to 6, and the red point $\boldsymbol{X}$ represents a test sample. The remaining black dots are training samples. According to kNN rule, the samples in the green round frame are the nearest neighbors of $\boldsymbol{X}$. While, according to improved kNN rule, samples in the blue and purple rectangular boxes are the nearest neighbors of $\boldsymbol{X}$ in the direction of variable 1 (namely x_1) and variable 2 (namely x_2), respectively. According to the above analysis, lower computational complexity is preferred for the improved kNN rule compared with traditional kNN rule.

3. The proposed fault isolation method

The main idea of the proposed method is shown in Fig. 3. Firstly, the nearest neighbors on each training sample space are obtained using the improved kNN rule along the direction of a specific variable, aiming to reduce computational complexity. The outlier-degree-based variable contributions are then calculated using the LOF of the variable. The contributions of other variables are obtained in the same way, among which the maximum one is selected as the isolation threshold value of the corresponding variable. In the process of online monitoring, the contribution of the monitored variables is calculated in real time. Once the contribution of variable is larger than the isolation threshold value, this variable is judged to be the dominant factor causing the corresponding sample faults. Finally, detailed derivation and analysis of isolability for fault variables are given in the presence of single and multiple fault variables.

The detailed procedures of the proposed fault isolation strategy are as follows:

Step 1. Finding the nearest neighbors along the direction of certain variable.

Along the direction of x_j^i (namely the direction of the jth variable), the nearest neighbor dataset $(N(\boldsymbol{X}^i) = [\boldsymbol{X}^{i1}, \boldsymbol{X}^{i2} \ldots \boldsymbol{X}^{il} \ldots \boldsymbol{X}^{iK}]^T)$ of sample $\boldsymbol{X}^i$ in offline dataset $\boldsymbol{X}$ based on the Euclidean distance is searched. The nearest neighbor dataset of every sample in the neighbors of the $\boldsymbol{X}^i$, that is $\boldsymbol{X}^{il}$, is computed as well.

Step 2. Calculating reachable distance and local reachability density.

The square of the Euclidean distance between the jth variable of $\boldsymbol{X}^{il}$ and that of its kth nearest neighbor $\boldsymbol{X}^{ilk}$ is obtained by

$$k_d^2\left(x_j^{il}\right) = \left(x_j^{il} - x_j^{ilk}\right)^2 \tag{12}$$

Then, the reachable distances between variable x_j^i of sample $\boldsymbol{X}^i$ and variable x_j^{il} of the lth nearest neighbor sample $\boldsymbol{X}^{il}$ $(l = 1, 2, \ldots, K)$ are expressed as:

$$R_d\left(x_j^i, x_j^{il}\right) = \sum_{l=1}^{K} \max\{k_d^2\left(x_j^{il}\right), d^2\left(x_j^i, x_j^{il}\right)\} \tag{13}$$

Meanwhile, the local reachability density ρ of variable x_j^i is calculated by

$$\rho(x_j^i) = \frac{1}{\frac{1}{K}\sum_{l=1}^{K} R_d\left(x_j^i, x_j^{il}\right)} \tag{14}$$

Step 3. Calculating local outlier factor.

The LOF of variable x_j^i which is treated as the contribution value of variable x_j^i is calculated by

$$c_{ij}^{LOF} = LOF(x_j^i) = \frac{1}{K}\frac{\Sigma_{l=1}^{K}\rho(x_j^{il})}{\rho(x_j^i)} \tag{15}$$

Remark 2. LOF is a classification method which is usually used for abnormal data analysis. If each object is assigned to a degree of being an outlier, this degree is called the LOF of the object. Inspired by this idea, a new variable contribution indicator is proposed based on outlier-degree of variable, which will be used to judge the possibility of a variable being the fault variable. The LOF of the variable is calculated by regarding the variable as a one-dimensional sample. Then the LOF value can be considered as the contribution of the variable, that is the so-called outlier-degree-based variable contributions. This makes it possible to achieve contribution-based fault variable isolation using the idea of LOF.

Step 4. Determining isolation threshold value.

The contribution of variable x_j^i in training dataset is calculated and the contribution matrix is achieved as

$$\begin{bmatrix} c_{11}^{LOF} & c_{12}^{LOF} & \cdots & c_{1j}^{LOF} & \cdots & c_{1m}^{LOF} \\ c_{21}^{LOF} & c_{22}^{LOF} & \cdots & c_{2j}^{LOF} & \cdots & c_{2m}^{LOF} \\ \vdots & \vdots & \ddots & \cdots & \ddots & \vdots \\ c_{i1}^{LOF} & c_{i2}^{LOF} & \cdots & c_{ij}^{LOF} & \cdots & c_{im}^{LOF} \\ \vdots & \vdots & \ddots & \vdots & \ddots & \vdots \\ c_{n1}^{LOF} & c_{n2}^{LOF} & \cdots & c_{nj}^{LOF} & \cdots & c_{nm}^{LOF} \end{bmatrix} \tag{16}$$

where c_{ij}^{LOF} represents the contribution of the jth variable x_j^i of the ith sample $\boldsymbol{X}^i$. The empirical method [14] is used to determine the isolation threshold value. Then, the isolation threshold value of each variable is selected by the maximum value of each column in the matrix in Eq. (16).

Remark 3. Generally, threshold value for one variable contribution is utilized to indicate the fluctuation of the variable contribution value under normal operating conditions. This signifies that the contributions of fault variables should be greater than contributions of the normal variables. The isolation threshold value of each variable is selected usually by the empirical method. The maximum contribution of corresponding variable among all the normal samples is chosen as the isolation threshold value. Therefore, the maximum value from each column of Eq. (16) is selected as the threshold value for the contribution of corresponding variable.

Step 5. Online fault isolation.

The $LOF(x_j^t)$ value of each variable $x_j^t (j = 1, 2, \ldots, m)$ for test sample $\boldsymbol{X}^t = (x_1^t, \ldots, x_m^t)$ is calculated by the same method in Eq. (17). Comparing the $LOF(x_j^t)$ value with the isolation threshold value, if $LOF(x_j^t)$ is greater than isolation threshold value, the variable x_j^t is considered to be a fault variable, otherwise it is a normal variable. The detailed expression of $LOF(x_j^t)$ is shown as:

$$\begin{aligned} LOF\left(x_j^t\right) &= \frac{1}{K}\frac{\Sigma_{l=1}^{K}\rho(x_j^{tl})}{\rho\left(x_j^t\right)} = \frac{R_d\left(x_j^t\right)}{K\sum_{l=1}^{K} R_d\left(x_j^{tl}\right)} \\ &= \begin{cases} \gamma_{x_j^{tl}}\sum_{l=1}^{K} d^2\left(x_j^t, x_j^{tl}\right), R_d\left(x_j^{tl}\right) < d^2\left(x_j^t, x_j^{tl}\right) \\ \gamma_{x_j^{tl}}\sum_{l=1}^{K} R_d\left(x_j^{tl}\right), R_d\left(x_j^{tl}\right) \geq d^2\left(x_j^t, x_j^{tl}\right) \end{cases} \\ &= \begin{cases} \gamma_{x_j^{tl}}\sum_{l=1}^{K}\left(x_j^t - x_j^{tl}\right)^2, \quad R_d\left(x_j^{tl}\right) < d^2\left(x_j^t, x_j^{tl}\right) \\ \gamma_{x_j^{tl}}\sum_{l=1}^{K}\left(\left(x_j^{tl} - x_j^{tlk}\right)^2\right), R_d\left(x_j^{tl}\right) \geq d^2\left(x_j^t, x_j^{tl}\right) \end{cases} \end{aligned} \tag{17}$$

with

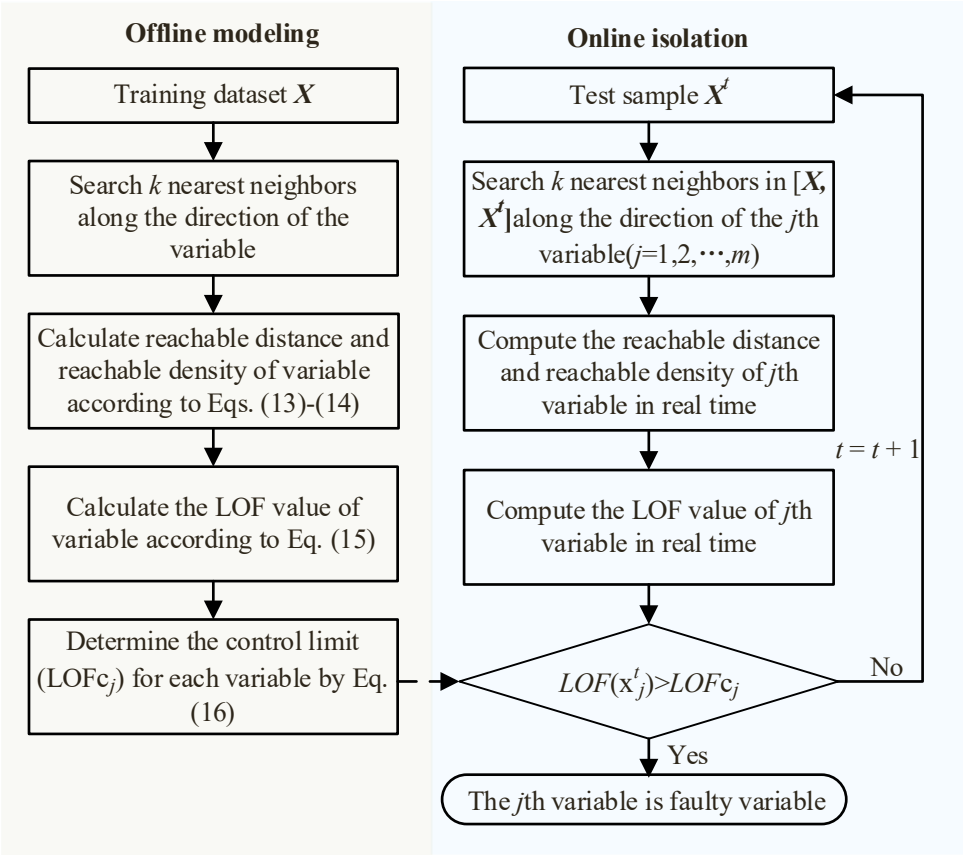

Fig. 4. The procedure of proposed fault isolation strategy.

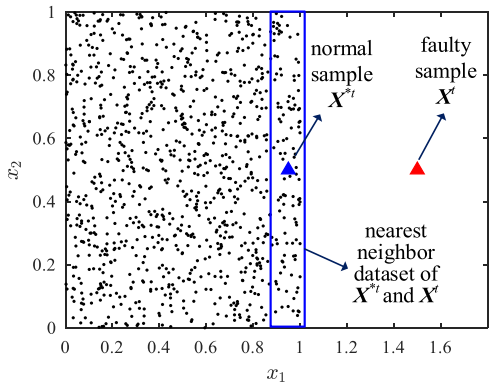

Fig. 5. Two-dimensional example for Case 1.

$$R_d\left(x_j^t\right) = \frac{1}{K}\sum_{l=1}^{K} R_d\left(x_j^t, x_j^{tl}\right) \tag{18}$$

$$R_d\left(x_j^{tl}\right) = \frac{1}{K}\sum_{l=1}^{K} R_d\left(x_j^{tl}, x_j^{tlk}\right) \tag{19}$$

where $\gamma_{x_j^{tl}} = K\sum_{l=1}^{K} R_d\left(x_j^{tl}\right)$ is a constant and x_j^{tlk} represents jth variable of kth nearest neighbor of $\boldsymbol{X}^{tl}$ along the direction of x_j^{tl}.

Remark 4. The contribution is computed by the local outlier factor of each variable, based on which a new fault isolation method with an explicit isolation threshold value is achieved. It is uninfluenced by the smearing effect since variable contribution defined in the original measurement space is only related to one corresponding variable and will not be affected by other variables. Then the impact of smearing effect can be reduced significantly.

The complete fault isolation procedure is presented in Fig. 4 including offline modeling and online isolation. The training dataset $\boldsymbol{X}$ consisting of offline samples $\boldsymbol{X}^i$ is used in offline modeling. The nearest neighbors of every sample are searched along the direction of the specific variable. Then, the reachable distance and reachable density of every variable in the sample are calculated according to Eqs. (13)-(14). The LOF values of variables are obtained by Eq. (15) and isolation threshold value is achieved by selecting the maximum one. In the process of online isolation, once the test sample is obtained, the nearest neighbors of the sample in the new dataset $[\boldsymbol{X}, \boldsymbol{X}^t]$ generated by adding the new test sample are searched along the specific variable direction. The reachable distance and reachable density of every variable in the sample are calculated, based on which the LOF value for every variable is obtained in real time. Comparing the LOF value of x_j^t with the corresponding isolation threshold value, if $LOF(x_j^t)$ is greater than the isolation threshold of x_j^t, the jth variableis regarded to be a fault variable. Otherwise, it is a normal variable.

It can be inferred from above procedures that the complexity of proposed method is largely related to the way neighbors are searched. Assuming that, in a high-dimensional space, d is the dimension of sample, and n is the number of training samples, then, computational complexity for each distance is $O(d)$. The computational complexity of traditional k-nearest neighbor is $O(dn^2)$. While the computational complexity of the improved k-nearest neighbor proposed in this paper is $O(n^2)$. Therefore, the computational complexity can be reduced significantly with the modified nearest neighbor rule.

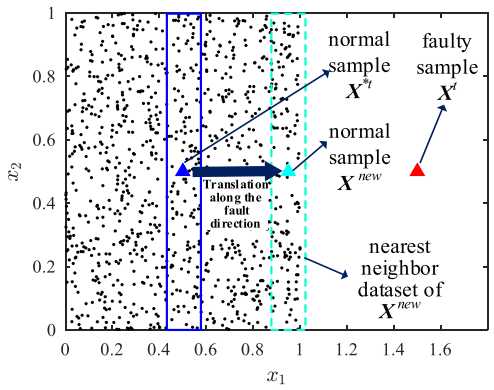

Fig. 6. Two-dimensional example for Case 2.

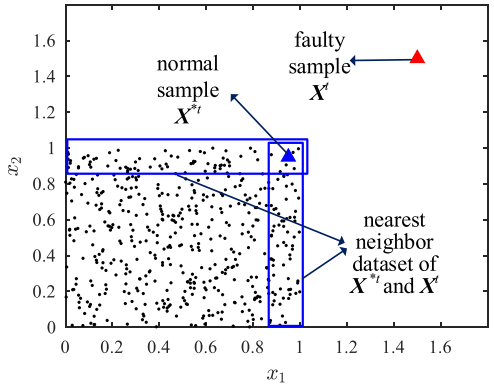

Fig. 7. Two-dimensional example for Case 3.

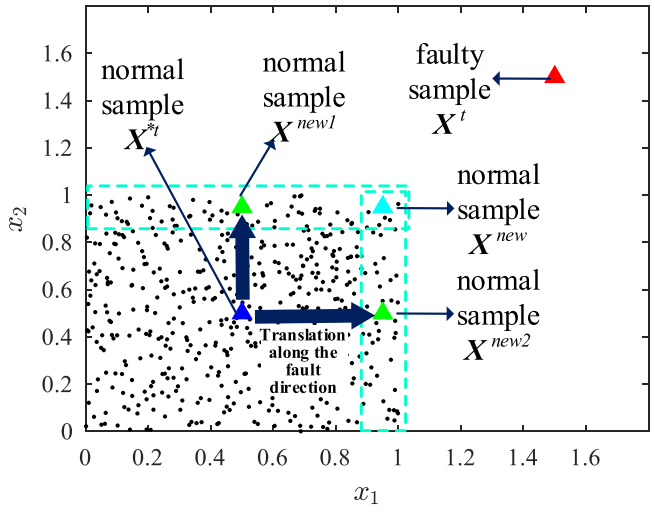

Fig. 8. Two-dimensional example for Case 4.

4. Isolability analysis of the proposed method

In this section, the isolability of the designed fault isolation method is analyzed considering the single and multiple additive faults.

4.1. Isolability analysis in the presence of the single additive fault

The isolability in the presence of the single fault is firstly analyzed and the additive fault is shown as

$$\boldsymbol{X}^t = \boldsymbol{X}^{*t} + \boldsymbol{\xi}_p f_p \tag{20}$$

where $\boldsymbol{X}^{*t}$ is the fault-free measurement, $\boldsymbol{\xi}_p$ is a column vector denoting fault direction (i.e., the pth column of the identity matrix), and f_p is fault magnitude. According to whether the nearest neighbor datasets of the faulty sample are the same as that of the normal sample, two cases are considered. In both cases, $\boldsymbol{\xi}_p$ is the same as the direction of fault variable x_1.

Case 1. In Fig. 5, along the direction of fault variable x_1, the faulty sample $\boldsymbol{X}^t$ (the red triangle) and the normal sample $\boldsymbol{X}^{*t}$ (the blue triangle) have the same nearest neighbor dataset, i.e., the samples in the blue rectangular box. The neighbor dataset is obtained along the direction of fault variable x_1. The other samples (the black dot '.') are normal samples. All samples in Figs. 5–8 are two-dimensional data, which can be expressed as (x_1, x_2).

According to Eq. (17) and assuming that the fault magnitude is much greater than the distance between a variable and its neighbors, i.e., $\left|f_p\right| \gg \left|x_j^{*t} - x_j^{tl}\right|$, the contribution value of variable x_j^t is obtained by

$$\begin{aligned} LOF\left(x_j^t\right) &= \gamma_{x_j^{tl}} \sum_{l=1}^{K} \left(x_j^{*t} - x_j^{tl} + \boldsymbol{\xi}_j^T \boldsymbol{\xi}_p f_p\right)^2 \\ &\approx \gamma_{x_j^{tl}} \sum_{l=1}^{K} \left(\boldsymbol{\xi}_j^T \boldsymbol{\xi}_p f_p\right)^2 \\ &= K\gamma_{x_j^{tl}} \left(\left(\boldsymbol{\xi}_p^T f_p\right)_i\right)^2 \\ &= \begin{cases} K\gamma_{x_j^{tl}} (f_p)^2, & p = j \\ 0, & p \neq j \end{cases} \end{aligned} \tag{21}$$

where $\gamma_{x_j^{tl}} = 1/K\sum_{l=1}^{K} R_d\left(x_j^{tl}\right)$ is a constant, $x_j^{*t} - x_j^{tl}$ is approximately zero due to same nearest neighbor dataset of faulty sample $\boldsymbol{X}^t$, and the normal sample $\boldsymbol{X}^{*t}$.

The premise of the approximate equation is that fault magnitude is much greater than the distance between a variable and its neighbors, i.e., $\left|f_p\right| \gg \left|x_j^{*t} - x_j^{tl}\right|$. Note that the difference $\left|x_j^{*t} - x_j^{tl}\right|$ is exceedingly tiny since fault-free part x_j^{*t} can be considered as normal values like x_j^{tl}, then above hypothesis is reasonable. Therefore, the result demonstrates that the contribution of fault variable is increased while that of normal variables almost unchanged in the case of single additive fault using the proposed method. Hence, it can be regarded that the smearing effect is reduced significantly.

Case 2. As shown in Fig. 6, along the direction of fault variable x_1, the faulty sample $\boldsymbol{X}^t$ (the red triangle) and the normal sample $\boldsymbol{X}^{*t}$ (the blue triangle) have different nearest neighbor dataset. Their nearest neighbor datasets are the samples in the blue and cyan rectangular box, respectively. The cyan triangle $\boldsymbol{X}^{new}$ is the sample after translation of $\boldsymbol{X}^{*t}$ along the fault variable x_1 direction. The other samples (the black dot '.') are normal samples.

The contribution value of variable x_j^t is calculated according to Eq. (17).

$$LOF(x_j^t) = \gamma_{x_j^{tl}} \sum_{l=1}^{K} \left(x_j^{*t} - x_j^{tl} + \boldsymbol{\xi}_j^T \boldsymbol{\xi}_p f_p\right)^2 \tag{22}$$

where $x_j^{*t} - x_j^{tl}$ is no longer approximately zero due to different nearest neighbor dataset of faulty sample $\boldsymbol{X}^t$ and the normal sample $\boldsymbol{X}^{*t}$. To eliminate redundant terms in Eq. (22), $\boldsymbol{X}^{*t}$ is translated along the direction of fault variable x_1. Then, $\boldsymbol{X}^{new}$ and faulty sample $\boldsymbol{X}^t$ have the same nearest neighbor dataset, i.e., the samples in the cyan rectangular box. The translation process is mathematically expressed in the following form

$$\boldsymbol{X}^t = \boldsymbol{X}^{new} + \boldsymbol{\xi}_p f_p^{new} \tag{23}$$

where

$$f_p^{new} = f_p - \boldsymbol{\xi}_p^T(\boldsymbol{X}^{new} - \boldsymbol{X}^t) \tag{24}$$

Then Eq. (18) can be transformed into the following form under the assumption that $\left|f_p^{new}\right| \gg \left|x_j^{new} - x_j^{tl}\right|$

$$\begin{aligned} LOF(x_j^t) = & \ \gamma_{x_j^{tl}} \sum_{l=1}^{K} \left(x_j^{new} - x_j^{tl} + \boldsymbol{\xi}_j^T \boldsymbol{\xi}_p f_p^{new}\right)^2 \\ \approx & \ \gamma_{x_j^{tl}} \sum_{l=1}^{K} \left(\boldsymbol{\xi}_j^T \boldsymbol{\xi}_p f_p^{new}\right)^2 \\ = & \ K\gamma_{x_j^{tl}} (\boldsymbol{\xi}_j^T \boldsymbol{\xi}_p f_p^{new})^2 \\ = & \begin{cases} K\gamma_{x_j^{tl}} (f_p^{new})^2 & , \ p = j \\ 0 & , p \neq j \end{cases} \end{aligned} \tag{25}$$

The derivation procedure and results are similar to Case 1. Therefore, the same conclusion can be inferred from Eq. (25).

4.2. Isolability analysis in the presence of the multiple additive faults

The isolability in the presence of the multiple variables fault is analyzed. For simplicity and without loss of generality, the case with two fault variables is analyzed. The fault is assumed as

$$\boldsymbol{X}^t = \boldsymbol{X}^{*t} + \boldsymbol{\xi}_p f_p + \boldsymbol{\xi}_q f_q \tag{26}$$

where $\boldsymbol{X}^{*t}$ is fault-free measurement, $\boldsymbol{\xi}_p$ and $\boldsymbol{\xi}_q$ are column vectors denoting fault direction (namely the pth, qth column of identity matrix), and f_p is fault magnitude. According to whether the nearest neighbor datasets of the faulty sample and the normal sample are the same, there are two cases. In the following two cases, $\boldsymbol{\xi}_p$ is the same as to the direction of fault variable x_1, $\boldsymbol{\xi}_q$ is the same as to the direction of fault variable x_2.

Case 3. In Fig. 7, along the direction of fault variables x_1 and x_2, the faulty sample $\boldsymbol{X}^t$ (the red triangle) and the normal sample $\boldsymbol{X}^{*t}$ (the blue triangle) have the same nearest neighbor dataset, respectively, i.e., the samples in two different blue rectangular boxes. The other samples (the black dot '.') are normal samples.

The contribution value of variable x_j^t is calculated according to Eq. (17).

$$\begin{aligned} LOF(x_j^t) = & \ \gamma_{x_j^{tl}} \sum_{l=1}^{K} \left(x_j^{*t} - x_j^{tl} + \boldsymbol{\xi}_j^T \boldsymbol{\xi}_p f_p + \boldsymbol{\xi}_j^T \boldsymbol{\xi}_q f_q\right)^2 \\ \approx & \ \gamma_{x_j^{tl}} \sum_{l=1}^{K} \left(\boldsymbol{\xi}_j^T \boldsymbol{\xi}_p f_p + \boldsymbol{\xi}_j^T \boldsymbol{\xi}_q f_q\right)^2), \left|f_p\right| \gg \left|x_j^{*t} - x_j^{tl}\right| and \left|f_q\right| \gg \left|x_j^{*t} - x_j^{tl}\right| \\ = & \ K\gamma_{x_j^{tl}} \left(\boldsymbol{\xi}_j^T \boldsymbol{\xi}_p f_p + \boldsymbol{\xi}_j^T \boldsymbol{\xi}_q f_q\right)^2 \\ = & \begin{cases} K\gamma_{x_j^{tl}} \left(f_p\right)^2 & , \ p = j \\ K\gamma_{x_j^{tl}} \left(f_q\right)^2 & , \ q = j \\ 0 & , p \neq j and q \neq j \end{cases} \end{aligned} \tag{27}$$

The approximate equation is based on the same hypothesis in the presence of the single additive fault. In the case of multiple additive faults, it can be observed that the contribution of fault variables increases while that of the normal variables is almost unchanged. Note that such a result can be applied to the case of three or more fault variables as well. Furthermore, it can be proven again that the variable contributions of multiple additive faults case are only related with corresponding variables. The smearing effect is reduced significantly.

Case 4. In Fig. 8, along the direction of fault variable x_1 and x_2, the faulty sample $\boldsymbol{X}^t$ (the red triangle) and the normal sample $\boldsymbol{X}^{*t}$ (the blue triangle) have different nearest neighbor dataset. The sample after translation of $\boldsymbol{X}^{*t}$ along the direction of fault variables x_1 and x_2 respectively is $\boldsymbol{X}^{new1}$, $\boldsymbol{X}^{new2}$ (the two green triangles). And the sample after two translations of $\boldsymbol{X}^{*t}$ along the direction of fault variables x_1 and x_2 is $\boldsymbol{X}^{new}$ (the cyan triangle). The other samples (the black dot '.') are normal samples.

The contribution value of variable x_j^t is calculated according to Eq. (17).

$$LOF(x_j^t) = \gamma_{x_j^{tl}} \sum_{l=1}^{K} \left(x_j^{*t} - x_j^{tl} + \boldsymbol{\xi}_j^T \boldsymbol{\xi}_p f_p + \boldsymbol{\xi}_j^T \boldsymbol{\xi}_q f_q\right)^2 \tag{28}$$

where $x_j^{*t} - x_j^{tl}$ is no longer approximately zero due to different nearest neighbor dataset of faulty sample $\boldsymbol{X}^t$ and the normal sample $\boldsymbol{X}^{*t}$. To eliminate redundant terms in Eq. (28), $\boldsymbol{X}^t$ is translated twice along the direction of fault variables x_1 and x_2. After the translation, the new sample $\boldsymbol{X}^{new}$ (the cyan triangle) and faulty sample $\boldsymbol{X}^t$ have the same nearest neighbor dataset, their nearest neighbor datasets are composed of the samples in the two cyan rectangular boxes as shown in Fig. 8, respectively. The translation process is mathematically expressed in the following form

$$\boldsymbol{X}^t = \boldsymbol{X}^{new} + \boldsymbol{\xi}_p f_p^{new} + \boldsymbol{\xi}_q f_q^{new} \tag{29}$$

$$f_p^{new} = f_p - \boldsymbol{\xi}_p^T(\boldsymbol{X}^{new1} - \boldsymbol{X}^{*t}), \quad f_q^{new} = f_q - \boldsymbol{\xi}_q^T(\boldsymbol{X}^{new2} - \boldsymbol{X}^{*t}) \tag{30}$$

Then Eq. (28) can be transformed into the following form

$$\begin{aligned} LOF(x_j^t) = & \ \gamma_{x_j^{tl}} \sum_{l=1}^{K} \left(x_j^{new} - x_j^{tl} + \boldsymbol{\xi}_j^T \boldsymbol{\xi}_p f_p^{new} + \boldsymbol{\xi}_j^T \boldsymbol{\xi}_q f_q^{new}\right)^2 \\ \approx & \ \gamma_{x_j^{tl}} \sum_{l=1}^{K} \left(\boldsymbol{\xi}_j^T \boldsymbol{\xi}_p f_p^{new} + \boldsymbol{\xi}_j^T \boldsymbol{\xi}_q f_q^{new}\right)^2, \\ = & \ K\gamma_{x_j^{tl}} (\boldsymbol{\xi}_j^T \boldsymbol{\xi}_p f_p^{new} + \boldsymbol{\xi}_j^T \boldsymbol{\xi}_q f_q^{new})^2 \\ = & \begin{cases} K\gamma_{x_j^{tl}} \left(f_p^{new}\right)^2 & , \ p = j \\ K\gamma_{x_j^{tl}} \left(f_q^{new}\right)^2 & , \ q = j \\ 0 & , p \neq j and q \neq j \end{cases} \end{aligned} \tag{31}$$

where $\left|f_p^{new}\right| \gg \left|x_j^{new} - x_j^{tl}\right| \& \left|f_q^{new}\right| \gg \left|x_j^{new} - x_j^{tl}\right|$..

The derivation procedure and result are similar to Case 3. Therefore, the same conclusion can be reached from Eq. (31).

5. Case studies

To evaluate the performance of the proposed fault isolation method, 2 cases are studied including a numerical example and the typical industrial process benchmark called Tennessee Eastman process.

5.1. Numerical example

The dataset under normal operating condition is generated by the model described in Eq. (32) [12].

$$\boldsymbol{X} = \begin{bmatrix} -0.3441 & 0.4815 & 0.6637 \\ -0.2313 & -0.5936 & 0.3545 \\ -0.5060 & 0.2495 & 0.0739 \\ -0.5552 & -0.2405 & -0.1123 \\ -0.3371 & -0.3822 & -0.6115 \\ -0.3877 & -0.3868 & 0.2045 \end{bmatrix} \begin{bmatrix} t_1 \\ t_2 \\ t_3 \end{bmatrix} + noise \tag{32}$$

where random variables t_1, t_2, and t_3 are within [0,1], [0, 1.6], and [0, 1.2], respectively. They are all uniformly distributed. The noise is nor-

Table 1
Comparison results of fault isolation rate for single fault.

Index	SPE	T^2	φ
CDC (%)	70.8	75.6	93.8
RBC (%)	91.6	62.4	95.2
The proposed method (%)	—	94.0	—

mally distributed with zero mean and variance of 0.2. The numbers of generated training data are 500. These training data are used to construct the fault isolation model and determine isolation threshold value.

To compared with other methods, several CA-based methods are also conducted including RBC and CDC methods. In these methods, the number of principal components is set to three, which can ensure that the rate of the contributions of the principal components is larger than 80 %. The statistic indices used to compute the variable contribution are T^2, SPE, and φ with a tolerance level equal to 5 % (i.e., $\alpha = 0.05$). The number of nearest neighbors is set to $K = k = 8$. The choice of the values of K and k is usually determined based on experience. If the value of K or k is too large, the computational complexity increases. If the value of K or k is too small, the isolation results will be greatly affected by noises. Therefore, a practical approach is to try different values of K or k on training data and determine an appropriate value by cross validation [32].

5.1.1. *Fault isolation result in the presence of single fault*

In the case of single fault, the fault is added by $\boldsymbol{X}^t = \boldsymbol{X}^{*t} + \boldsymbol{\xi}_p f_p$, where the fault direction $\boldsymbol{\xi}_p$ is uniformly distributed among the six possible directions and the fault magnitude f_p is a random number uniformly distributed in the range of [0,5]. The uniformly distributed $\boldsymbol{\xi}_p$ represents any one variable possibly as a fault variable. The uniformly distributed f_p denotes that the fault magnitude is practically and more likely to be a random value rather than a fixed value. Similar settings can be found in other references [12,14]. Under this assumption, 500 fault samples are generated.

The fault isolation performance of different methods is shown in Table 1.

Table 2
Fault isolation rate for multiple faults.

Index	SPE	T^2	φ
CDC (%)	6.4	4.2	7.8
RBC (%)	15.0	18.6	51.2
The proposed method (%)	—	86.0	—

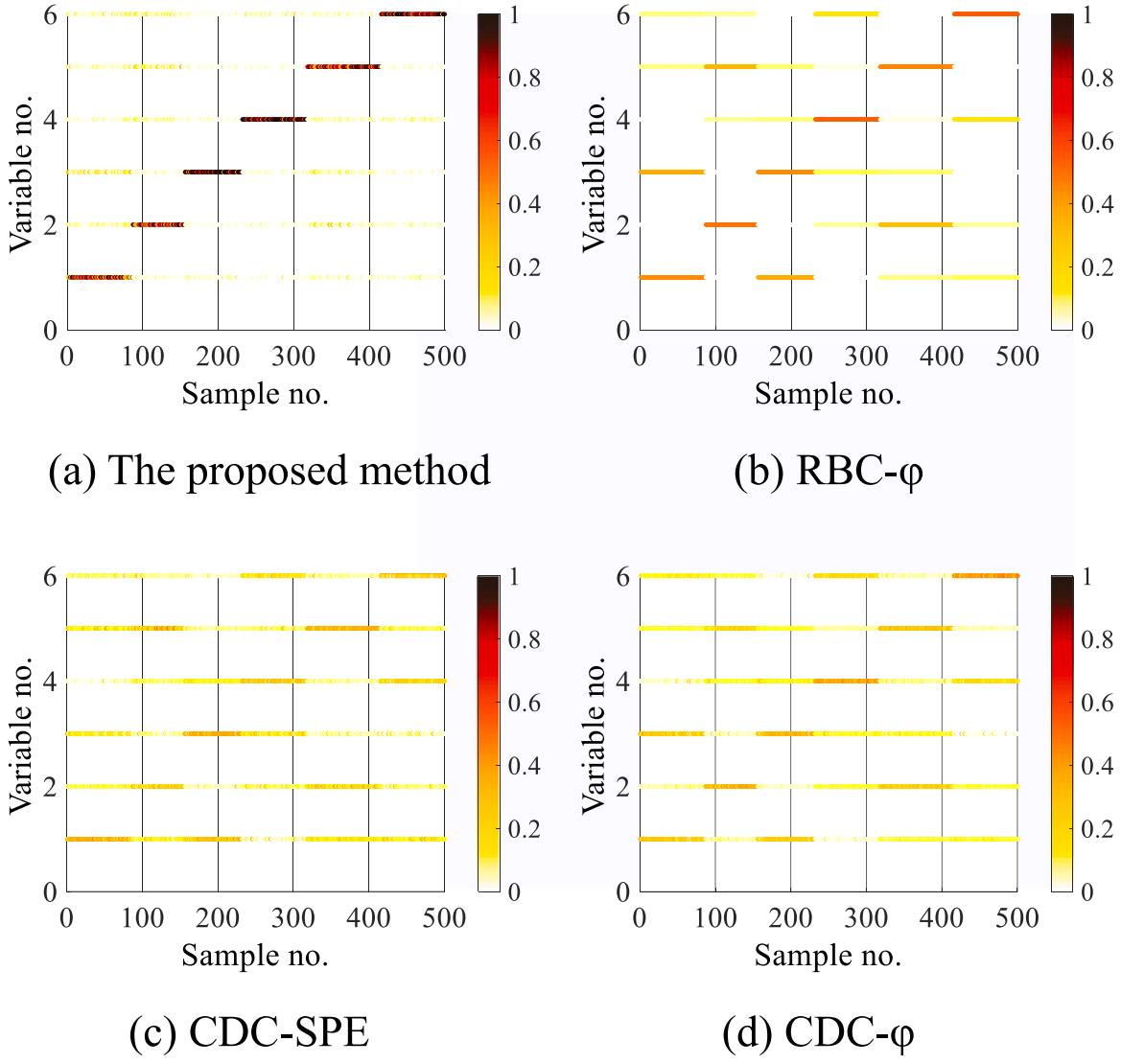

Fig. 9. Fault isolation results of variables 1 to 6 using different methods.

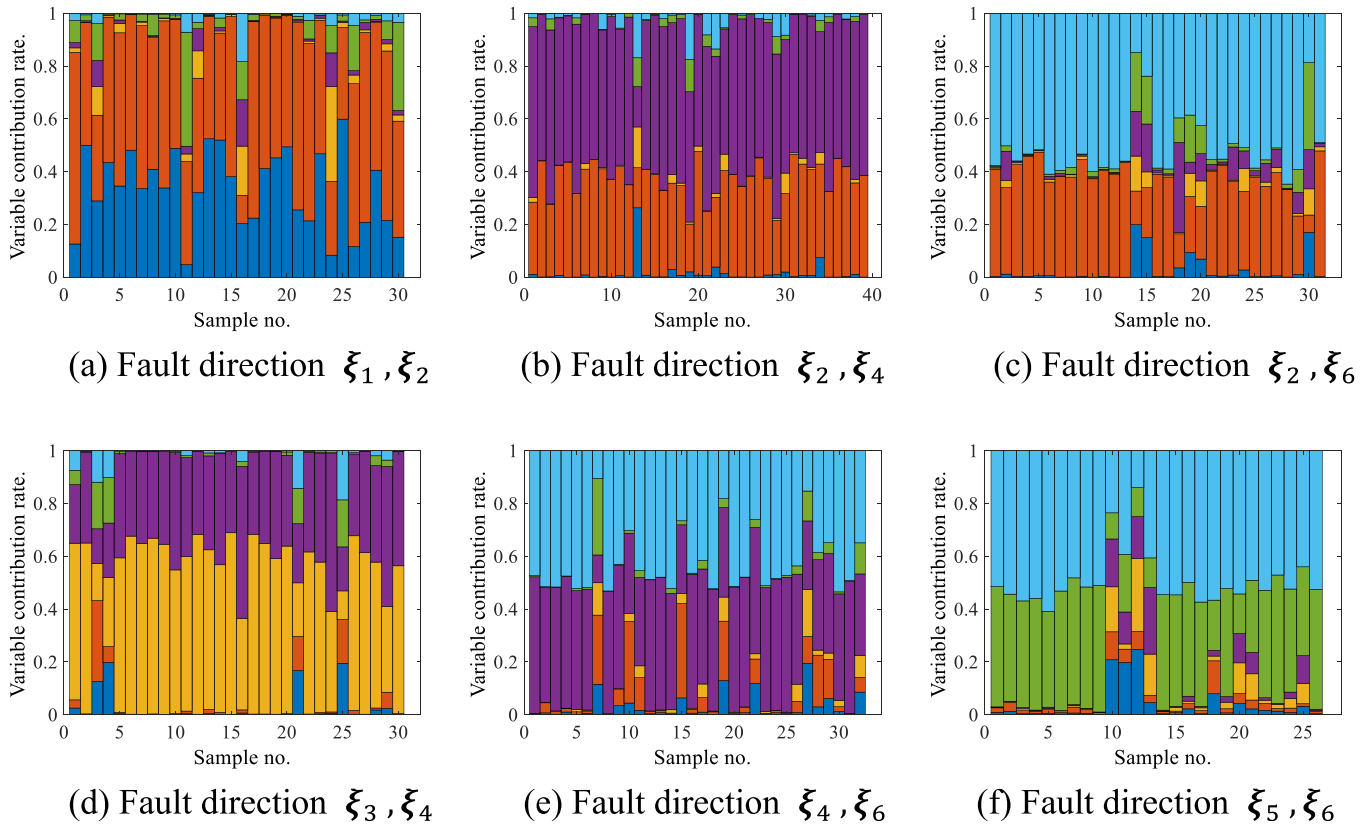

Fig. 10. Fault isolation results of variables 1–6 using the proposed method.

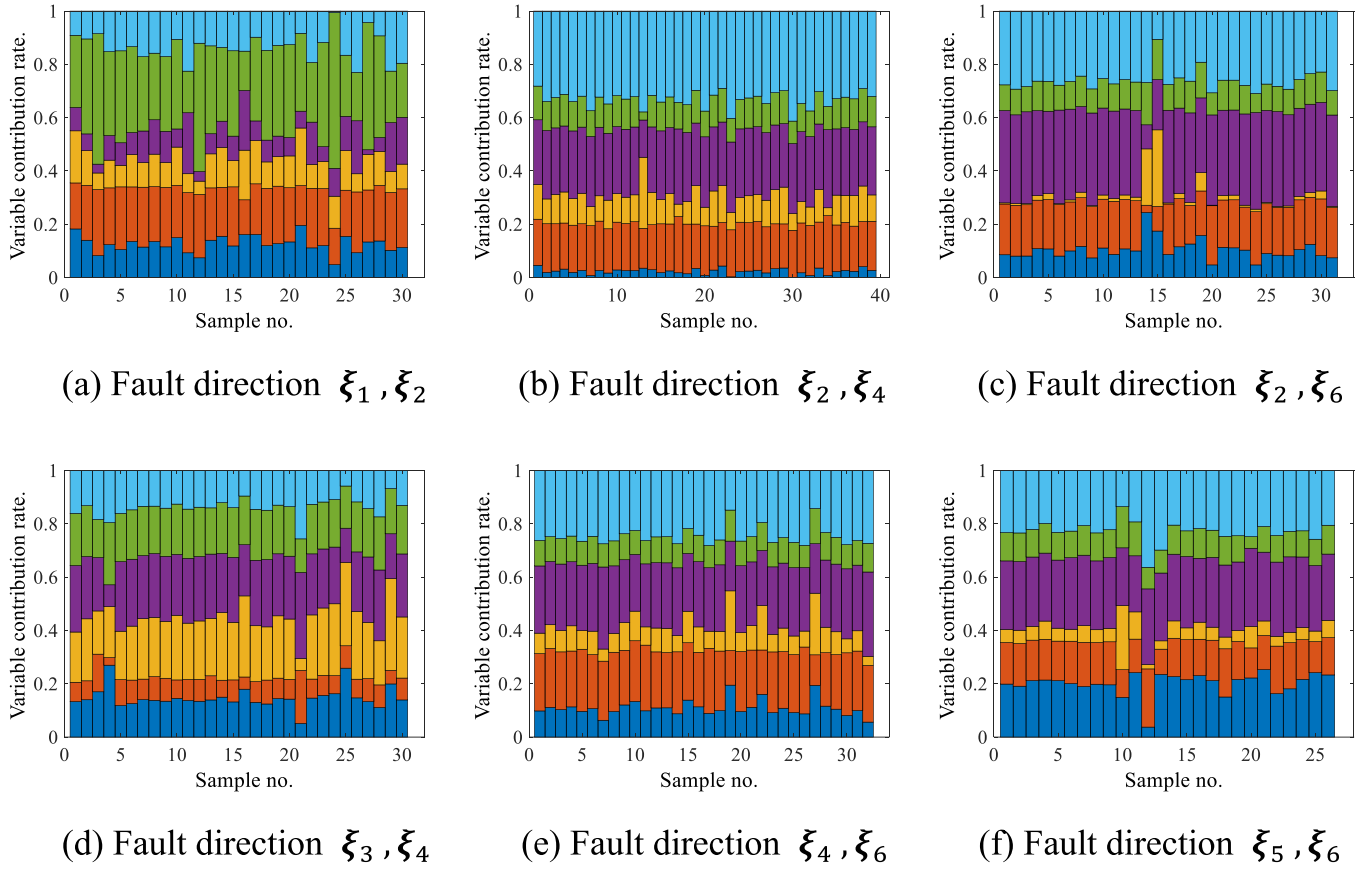

Fig. 11. Fault isolation results of variables 1–6 using the CDC-φ method.

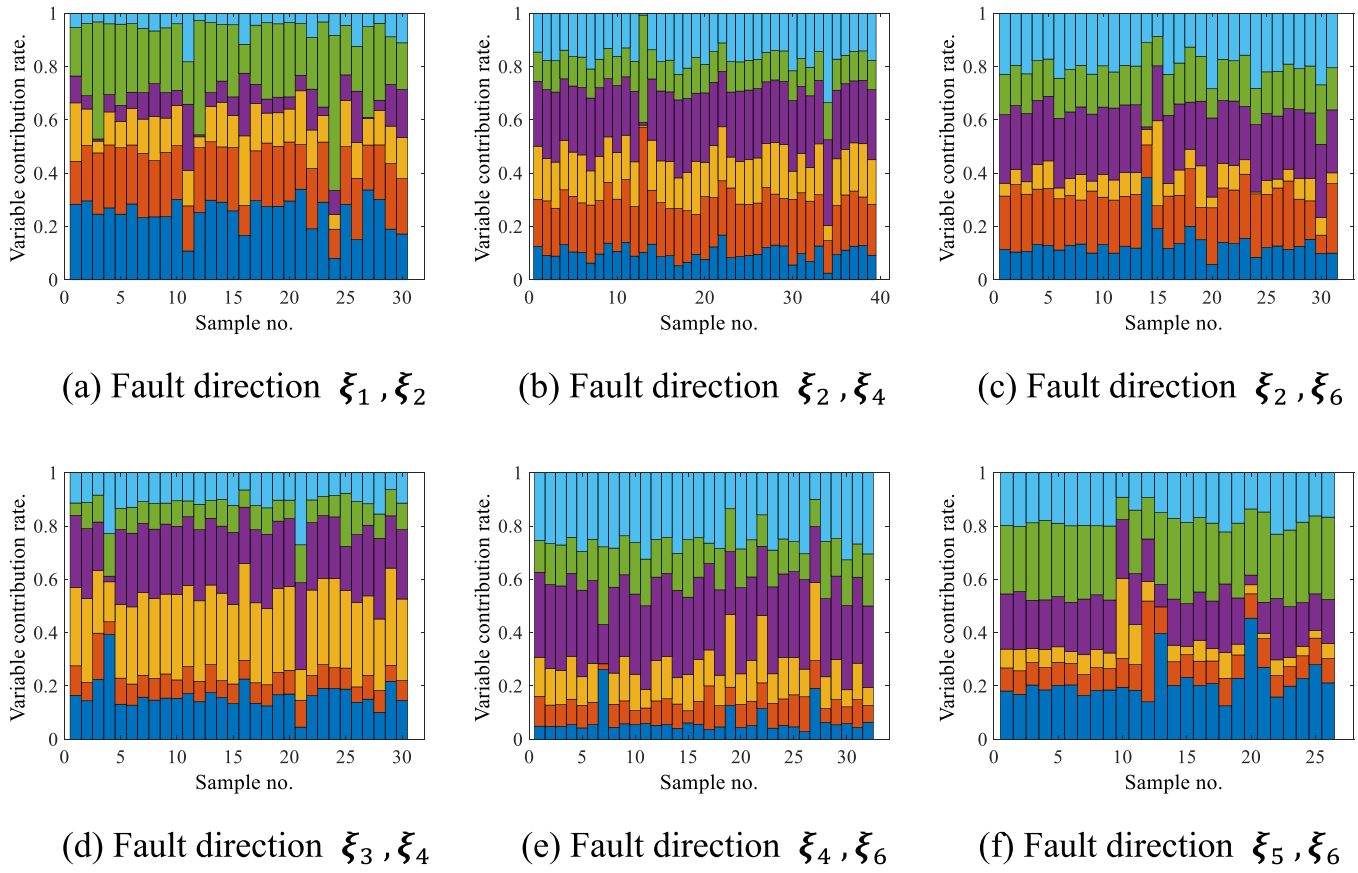

Fig. 12. Fault isolation results of variables 1–6 using the RBC-φ method.

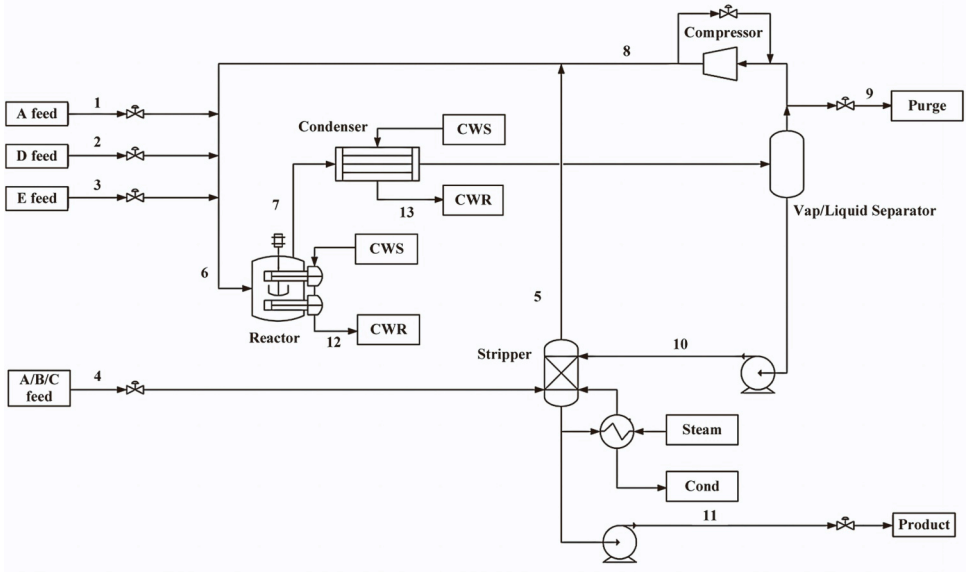

Fig. 13. The Tennessee Eastman process flowsheet [35].

In Table 1, the fault isolation rate (FIR) is used to assess the performance of these methods. The value of FIR is computed by diving the number of the correctly isolated samples X_{ci} by the number of the fault samples X_{total}, i.e., FIR $= \frac{X_{ci}}{X_{total}}$. When the RBC with SPE is applied to identify fault variables, 458 samples are correctly isolated. Hence, the FIR of the RBC-SPE is obtained by $458/500 = 91.6\%$, which is shown in row 3 and column 2 of Table 1. It can be observed that the FIRs of the CDC with SPE, CDC with T^2, and RBC with T^2 are 70.8 %, 75.6 %, and 62.4 %, respectively. The FIRs of the CDC with φ, RBC with SPE, RBC with φ, and the proposed method are 93.8 %, 91.6 %, 95.2 %, and 94 %, respectively. In summary, the proposed method has good isolation performance in the case of a single fault.

In the 500 fault samples, the number of fault samples caused by variables 1 to 6 is 86, 69, 76, 86, 98, 85, respectively. The isolation

Table 3
Fault description for the Tennessee Eastman process.

Fault No.	Description	Type
1	A/C feed ratio, B composition constant (Stream 4)	Step
2	B composition, A/C ratio constant (Stream 4)	
3	D feed temperature (Stream 2)	
4	Reactor cooling water inlet temperature	
5	Condenser cooling water inlet temperature	
6	A feed loss (Stream 1)	
7	C header pressure loss — reduced availability (Stream 4)	
8	A, B, C feed composition (Stream 4)	Random variation
9	D feed temperature (Stream 2)	
10	C feed temperature (Stream 4)	
11	Reactor cooling water inlet temperature	
12	Condenser cooling water inlet temperature	
13	Reaction kinetics	Slow drift
14	Reactor cooling water valve	Sticking
15	Condenser cooling water valve	
16	Unknown	Unknown
17	Unknown	
18	Unknown	
19	Unknown	
20	Unknown	
21	The valve for Stream 4 was fixed at the steady state position	Constant position

results of fault variables under different methods including RBC with φ, CDC with SPE, CDC with φ, and the proposed method are shown in Fig. 9.

In Fig. 9(c), it can be observed that many non-fault variables are incorrectly isolated as the fault variables in the CDC with SPE method, which results in the low FIR value as shown in Table 1. In Fig. 9(b) and (d), the contributions of certain fault variable and certain non-fault variable (such as the fault variable 1 and non-fault variable 3 in the first 86 samples) are very close due to the smearing effect, although the FIR value of RBC-φ and CDC-φ is highly reached to 95.2 % and 93.8 %. The comparison results of fault isolation show that the performance of the proposed method is better than the traditional methods since the smearing effect is reduced. The results are consistent with the theoretical analysis.

5.1.2. Fault isolation result in the presence of multiple faults

In the case of multiple faults, the fault is added by $\boldsymbol{X}^{t} = \boldsymbol{X}^{*t} + \boldsymbol{\xi}_p f_p + \boldsymbol{\xi}_q f_q$. The fault direction $\boldsymbol{\xi}_p$ and $\boldsymbol{\xi}_q$ are both uniformly distributed among the six possible directions. The fault magnitude f_p and f_q are both random numbers uniformly distributed in the range of [0,5]. Under this assumption, 500 fault samples are generated by the model. The fault isolation results are shown in Table 2 and Fig. 10.

In these 500 fault samples, the number of samples (NoS) with fault direction $\boldsymbol{\xi}_1$ and $\boldsymbol{\xi}_2$ is 30, NoS with fault direction $\boldsymbol{\xi}_2$ and $\boldsymbol{\xi}_4$ is 39, NoS with fault direction $\boldsymbol{\xi}_2$ and $\boldsymbol{\xi}_6$ is 31, NoS with fault direction $\boldsymbol{\xi}_3$ and $\boldsymbol{\xi}_4$ is 30, NoS with fault direction $\boldsymbol{\xi}_4$ and $\boldsymbol{\xi}_6$ is 32, and NoS with fault direction $\boldsymbol{\xi}_5$ and $\boldsymbol{\xi}_6$ is 26. The contribution of variables 1 to 6 is indicated respectively in dark blue, orange, yellow, purple, green and light blue in Fig. 10, Fig. 11, and Fig. 12.

In the case that multiple faults occurred simultaneously, the fault isolation is achieved only when all fault variables of a sample are isolated, that is, all the contribution values of the fault variables are greater than the isolation threshold value. Isolation results of fault variables under different methods including the proposed method, CDC with φ, and RBC with φ are shown in Figs. 10, 11, and 12, respectively. The fault variables can be easily isolated in Fig. 10 according to the variable contribution rate. While in the other two methods as shown in Figs. 11–12, the contribution rate of the fault variables and some normal variables are close which is hard for fault isolation. The results of fault isolation in Table 2 show that the FIR of the proposed method is 86.0 %, which is much better than the traditional methods.

5.2. TE process analysis

The TE process is widely used to evaluate the performance of the fault detection algorithms [35–37]. Five operating units, including a reactor, a condenser, a compressor, a separator, and a stripper are included in the TE process [38]. Two liquid products, G and H, are produced from gaseous reactants A, B, C, E and inert gases B, as shown in Fig. 13. Dataset contains 21 faults, as presented in Table 3 [35], and each sample of dataset contains 52 variables. These variables can be used for fault isolation. In this experiment, the datasets in the case of fault 1 and fault 7 are used to evaluate the performance of the proposed fault isolation method. The fault type of these two datasets is step fault, which belongs to additive fault. According to the theoretical analysis in Section 4, the fault variables of fault 1 and fault 7 can be isolated. 960 samples in the training dataset are generated under normal operation condition, which are used to determine the isolation threshold value. 800 faulty samples in the case of fault 1 and fault 7 are used as test sets, respectively.

To compare with other methods, several CA-based methods are also

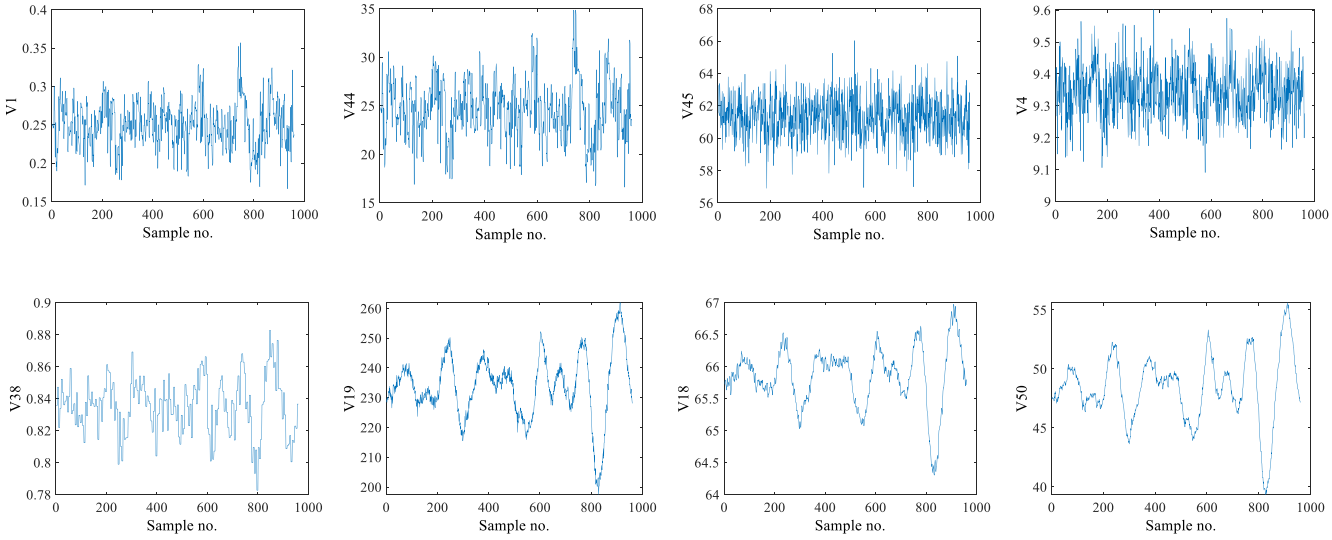

Fig. 14. The actual distribution situation of variables before fault 1 occurrence.

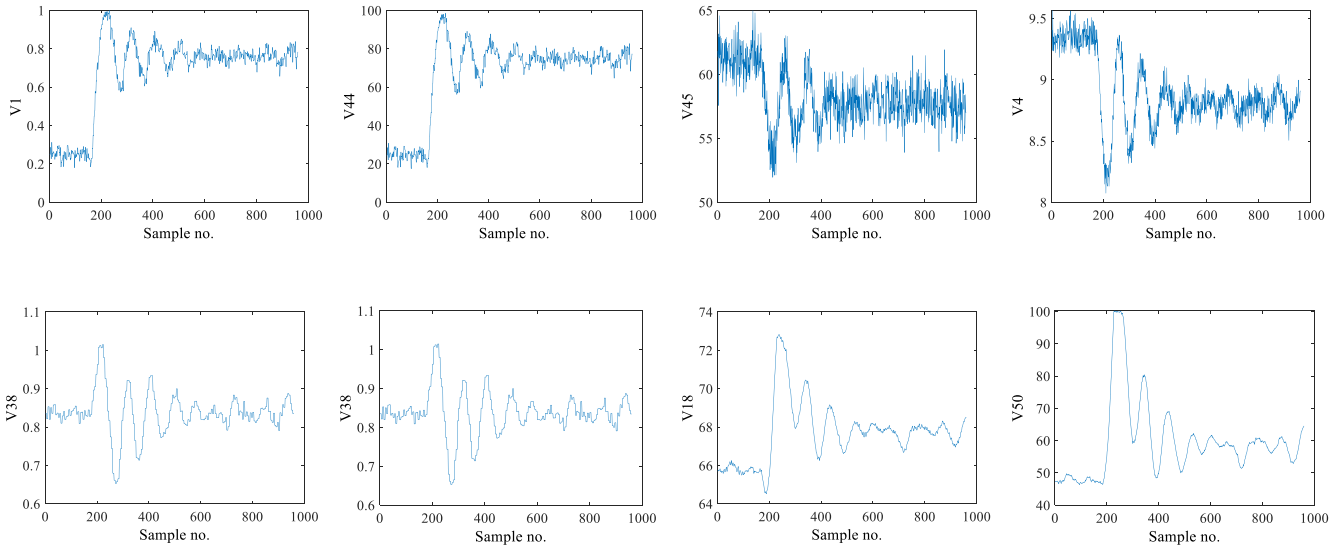

Fig. 15. The actual distribution situation of variables after fault 1 occurrence.

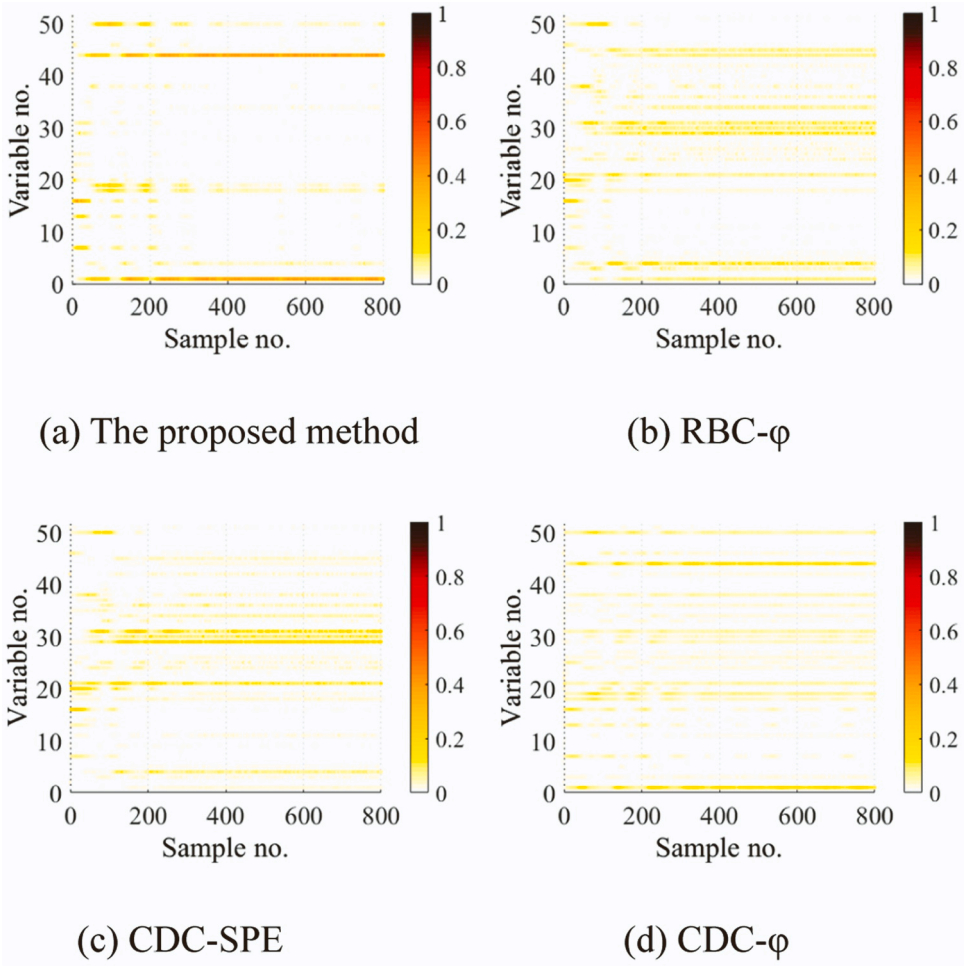

Fig. 16. Fault isolation results in the case of fault 1 using different methods.

conducted including RBC and CDC. In these methods, the number of principal elements is selected being 31 (i.e., the contribution rate>90 %). In the proposed method, the number of nearest neighbors is selected as $K = k = 14$, and the remaining parameters are the same as the numerical simulation.

In the case of fault 1, the system is in the open-loop control, the ratio between the reactants A and C changed, which sequentially affects 44th variable, 1st variable, 45th variable, 4th variable, 38th variable, 19th

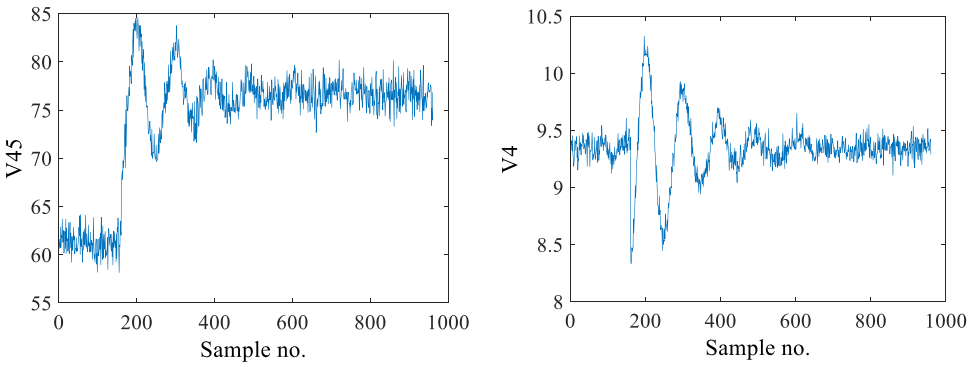

Fig. 17. The actual distribution situation of 45th variable and 4th variable after fault 7 occurrence.

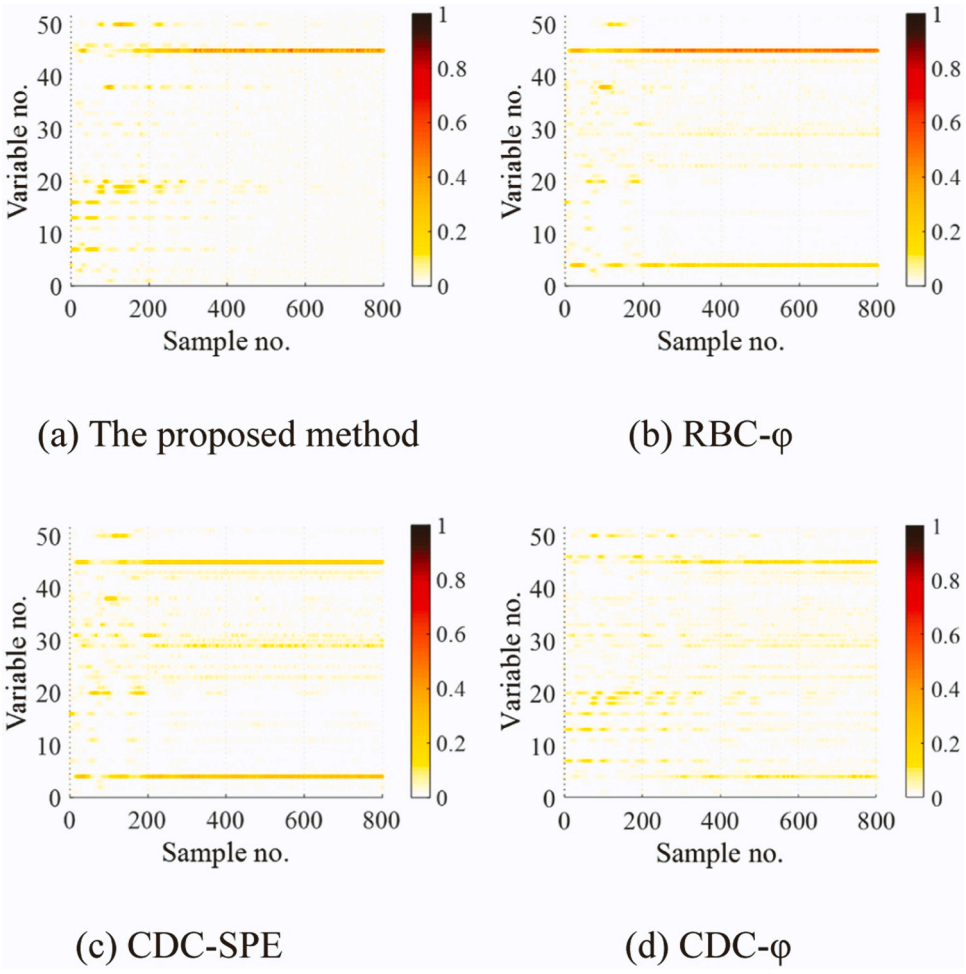

Fig. 18. Fault isolation results in the case of fault 7 using different methods.

variable, 18th variable, and 50th variable [4]. The actual distribution situation of these variables before and after occurrence of fault 1 are shown in Fig. 14 and Fig. 15, respectively. Note that there are 960 samples in total, faults were introduced after the 160th sample in Figs. 14 and 15.

Fig. 16 shows the variable isolation result in the presence of fault 1. Using these traditional CA-based methods including RBC-φ, CDC-SPE, and CDC-φ, error isolation can be observed due to the smearing effect. For instance, the 29th, 30th, 31st variable in the RBC-φ method is incorrectly isolated. While the proposed method is not affected by the smearing effect. Therefore, the proposed method can accurately isolate the variables including the 1st and 44th variable as shown in Fig. 16(a).

Fault 7 is caused by the C header pressure loss without change of any compositions in the stream [4]. The C header pressure is determined by the open position of the feed flow valve of Stream 4, i.e., 45th variable. Hence, the 45th variable would be the only variable influenced by fault 7. The actual distribution situation of 45th variable and 4th variable which are strongly correlated after occurrence of fault 7 are shown in Fig. 17.

Fig. 18 shows the result of variable isolation in the presence of fault 7. Variable 4 is isolated as fault variable by the CDC-SPE method since variable 4 and variable 45 have strong correlation, resulting in false isolation as shown in Fig. 18(c). In Fig. 18(d), the fault variable can hardly be distinguished. While the proposed method is not affected by

the smearing effect. The fault variable (i.e., the 45th variable) can be accurately isolated by the proposed method as shown in Fig. 18(a).

6. Conclusion

In this paper, a novel fault isolation method using outlier-degree-based variable contributions is proposed. The variable contribution indicator is defined from the perspective of spatial distance. The smearing effect is mitigated significantly compared with traditional CA-based fault isolation approaches. The detailed derivation and analysis of isolability for fault variables illustrate that the proposed method can isolate single fault variable or multiple fault variables. Case studies on numerical examples and the Tennessee Eastman process demonstrate the effectiveness of the proposed fault isolation method. The proposed method exhibits better isolation performance for fault variables, which can effectively improve the fault diagnosis effect of industrial processes. In future work, identification of the magnitude and shape of the fault is worth studying after isolating the fault variables.

CRediT authorship contribution statement

Xianghong Xue: Writing – review & editing, Supervision, Project administration, Methodology, Investigation, Funding acquisition, Formal analysis. **Qingliang Li:** Writing – review & editing, Visualization, Validation, Software, Methodology, Investigation, Formal analysis, Data curation. **Lingxia Mu:** Writing – review & editing, Writing – original draft, Supervision, Resources, Project administration, Methodology, Investigation, Funding acquisition, Formal analysis, Conceptualization. **Wenzhe Sun:** Writing – review & editing, Writing – original draft, Visualization, Validation, Software, Methodology, Investigation, Formal analysis, Data curation. **Youmin Zhang:** Writing – review & editing, Supervision, Resources, Project administration, Investigation, Funding acquisition, Formal analysis, Conceptualization. **Nan Feng:** Writing – review & editing, Visualization, Validation, Software, Methodology, Investigation, Formal analysis.

Declaration of Competing Interest

The authors declare that they have no known competing financial interests or personal relationships that could have appeared to influence the work reported in this paper.

Acknowledgements

This work was supported by the National Natural Science Foundation of China (No. 62373299, No. 62127809, and No. 61833013), Key R&D Program of Shaanxi Province (No. 2024GX-YBXM-093), and China Postdoctoral Science Foundation (No. 2022MD723834).

References

[1] Pilario KES, Cao Y. Canonical variate dissimilarity analysis for process incipient fault detection. IEEE Trans Ind Inform 2018;14(12):5308–15. https://doi.org/10.1109/TII.2018.2810822.
[2] Chen Z, Li X, Yang C, Peng T, Yang C, Karimi H, Gui W. A data-driven ground fault detection and isolation method for main circuit in railway electrical traction system. ISA Trans 2019;87:264–71. https://doi.org/10.1016/j.isatra.2018.11.031.
[3] Yan Z, Kuang T, Yao T. Multivariate fault isolation of batch processes via variable selection in partial least squares discriminant analysis. ISA Trans 2017;70:389–99. https://doi.org/10.1016/j.isatra.2017.06.014.
[4] Liu J. Fault diagnosis using contribution plots without smearing effect on non-faulty variables. J Process Control 2012;22(9):1609–23. https://doi.org/10.1016/j.jprocont.2012.06.016.
[5] Lahdhiri H, Taouali O. Reduced rank KPCA based on GLRT chart for sensor fault detection in nonlinear chemical process. Measurement 2021;169:108342. https://doi.org/10.1016/j.measurement.2020.108342.
[6] Márquez-Vera MA, López-Ortega O, Ramos-Velasco LE, Rodríguez A, Ramos-Fernández JC, Hernández-Salazar JA. Adaptive threshold PCA for fault detection and isolation. J Robot Control 2021;2(3):119–25. https://doi.org/10.18196/jrc.2364.
[7] Li CC, Jeng JC. Multiple sensor fault diagnosis for dynamic processes. ISA Trans 2010;49(4):415–32. https://doi.org/10.1016/j.isatra.2010.05.001.
[8] Liu J, Chen D. Fault isolation using modified contribution plots. Comput Chem Eng 2014;61(2)):9–19. https://doi.org/10.1016/j.compchemeng.2013.10.004.
[9] Li G, Alcala CF, Qin SJ, Zhou D. Generalized reconstruction-based contributions for outpour relevant fault diagnosis with application to the Tennessee Eastman process. IEEE Trans Control Syst Technol 2011;19(5):1114–27. https://doi.org/10.1109/TII.2018.2810822.
[10] Zheng Y, Mao S, Liu S, Wong SH, Wang Y. Normalized relative RBC-based minimum risk Bayesian decision approach for fault diagnosis of industrial process. IEEE Transaction. Ind Electron 2016;63(12):7723–32. https://doi.org/10.1109/TIE.2016.2591902.
[11] He B, Yang X, Chen T, Zhang J. Reconstruction-based multivariate contribution analysis for fault isolation: A branch and bound approach. J Process Control 2012;22(7):1228–36. https://doi.org/10.1016/j.jprocont.2012.05.010.
[12] Alcala CF, Qin SJ. Analysis and generalization of fault diagnosis methods for process monitoring. J Process Control 2011;21(3):322–30. https://doi.org/10.1016/j.jprocont.2010.10.005.
[13] Van den Kerkhof P, Vanlaer J, Gins G, Van Impe JFM. Analysis of smearing-out in contribution plot based fault isolation for statistical process control. Chem Eng Sci 2013;104:285–93. https://doi.org/10.1016/j.ces.2013.08.007.
[14] Zhou Z, Wen C, Yang C. Fault isolation based on k-nearest neighbor rule for industrial processes. IEEE Trans Ind Electron 2016;63(4):2578–86. https://doi.org/10.1109/TIE.2016.2520898.
[15] Alcala CF, Qin JS. Reconstruction-based contribution for process monitoring. Automatica 2009;45(7):1593–600. https://doi.org/10.1016/j.automatica.2009.02.027.
[16] Sun CY, Yin YZ, Kang HB, Ma HJ. A distributed principal component regression method for quality-related fault detection and diagnosis. Inf Sci 2022;600:301–22. https://doi.org/10.1016/j.ins.2022.03.069.
[17] Tao Y, Shi H, Song B, Tan S. A novel dynamic weight principal component analysis method and hierarchical monitoring strategy for process fault detection and diagnosis. IEEE Trans Ind Electron 2020;67(9):7994–8004. https://doi.org/10.1109/TIE.2019.2942560.
[18] Liu Y, Zeng J, Xie L, Luo S, Su H. Structured joint sparse principal component analysis for fault detection and isolation. IEEE Trans Ind Inform 2019;15(5):2721–31. https://doi.org/10.1109/TII.2018.2868364.
[19] Wang JX, Wang ZW, Stetsyuk V, Ma XZ, Gu FS, Li WH. Exploiting Bayesian networks for fault isolation: A diagnostic case study of diesel fuel injection system. ISA Trans 2019;86:276–86. https://doi.org/10.1016/j.isatra.2018.10.044.
[20] Bai YQ, Wang JZ. Fault detection and isolation using relative information for multi-agent systems. ISA Trans 2021;116:182–90. https://doi.org/10.1016/j.isatra.2021.01.030.
[21] Cervantes-Bobadilla M, García-Morales J, Saavedra-Benítez YI, Hernández-Pérez JA, Adam-Medina M, Guerrero-Ramírez GV, Escobar-Jímenez RF. Multiple fault detection and isolation using artificial neural networks in sensors of an internal combustion engine. Eng Appl Artif Intell 2023;117:105524. https://doi.org/10.1016/j.engappai.2022.105524.
[22] Khan AS, Khan AQ, Iqbal N, Mustafa G, Abbasi MA, Mahmood A. Design of a computationally efficient observer-based distributed fault detection and isolation scheme in second-order networked control systems. ISA Trans 2022;128:229–41. https://doi.org/10.1016/j.isatra.2021.09.004.
[23] Wang G, Liu J, Li Y. Fault diagnosis using kNN reconstruction on MRI variables. J Chemom 2015;29(7):399–410. https://doi.org/10.1002/cem.2719.
[24] Yu J, Jang J, Yoo J, Park JH, Kim S. A fault isolation method via classification and regression tree-based variable ranking for drum-type steam boiler in thermal power plant. Energies 2018;11(5):1142. https://doi.org/10.3390/en11051142.
[25] Breunig MM, Kriegel HP, Ng RT, Sander J. LOF: Identifying density-based local outliers. Proc 2000 ACM SIGMOD Int Conf Manag Data 2000;29:93–104. https://doi.org/10.1145/342009.335388.
[26] Zhu J, Wang Y, Zhou D, Gao F. Batch process modeling and monitoring with local outlier factor. IEEE Trans Control Syst Technol 2019;27(4):1552–65. https://doi.org/10.1109/TCST.2018.2815545.
[27] Chen ZH, Xu K, Wei JW, Dong GZ. Voltage fault detection for lithium-ion battery pack using local outlier factor. Measurement 2019;146:544–56. https://doi.org/10.1016/j.measurement.2019.06.052.
[28] Lee J, Kang B, Kang S-H. Integrating independent component analysis and local outlier factor for plant-wide process monitoring. J Process Control 2011;21(7):1011–21. https://doi.org/10.1016/j.jprocont.2011.06.004.
[29] Ma H, Hu Y, Shi H. Fault detection and identification based on the neighborhood standardized local outlier factor method. Ind Eng Chem Res 2013;52(6):2389–402. https://doi.org/10.1021/ie302042c.
[30] Lee WJ, Mendis GP, Triebe MJ. Monitoring of a machining process using kernel principal component analysis and kernel density estimation. J Intell Manuf 2020;31:1175–89. https://doi.org/10.1007/s10845-019-01504-w.
[31] Gonzalez R, Huang B, Lau E. Process monitoring using kernel density estimation and Bayesian networking with an industrial case study. ISA Trans 2015;58:330–47. https://doi.org/10.1016/j.isatra.2015.04.001.
[32] He QP, Wang J. Fault detection using the k-nearest neighbor rule for semiconductor manufacturing processes. IEEE Trans Semicond Manuf 2007;20(4):345–54. https://doi.org/10.1109/TSM.2007.907607.
[33] Zhou Z, Wen C, Yang C. Fault detection using random projections and k-nearest neighbor rule for semiconductor manufacturing processes. IEEE Trans Semicond Manuf 2015;28(1):70–9. https://doi.org/10.1109/TSM.2014.2374339.

[34] Zhang C, Gao XW, Xu T, et al. Fault detection strategy of independent component-based k nearest neighbor rule. Control Theory Appl 2018;35(6):805–12. https://doi.org/10.7641/CTA.2017.70394.
[35] Rato TJ, Reis MS. Fault detection in the Tennessee Eastman benchmark process using dynamic principal components analysis based on decorrelated residuals (DPCA-DR). Chemom Intell Lab Syst 2013;125:101–8. https://doi.org/10.1016/j.chemolab.2013.04.002.
[36] Hajihosseini P, Anzehaee MM, Behnam B. Fault detection and isolation in the challenging Tennessee Eastman process by using image processing techniques. ISA Trans 2018;79:137–46. https://doi.org/10.1016/j.isatra.2018.05.002.
[37] Lahdhiri H, Taouali O. Interval valued data driven approach for sensor fault detection of nonlinear uncertain process. Measurement 2021;171:108776. https://doi.org/10.1016/j.measurement.2020.108776.
[38] Russell EL, Chiang LH, Braatz RD. Fault detection in industrial processes using canonical variate analysis and dynamic principal component analysis. Chemom Intell Lab Syst 2000;51(1):81–93. https://doi.org/10.1016/S0169-7439(00)00058-7.